Structural changes in model oxide catalysts studied by operando XAFS

Gajdek-Vivar, Dorotea

2024

Document Version:
Peer reviewed version (aka post-print)

Link to publication

Citation for published version (APA):
Gajdek-Vivar, D. (2024). *Structural changes in model oxide catalysts studied by operando XAFS*. [Doctoral Thesis (compilation), Lund University]. Lund University.

Total number of authors:
1

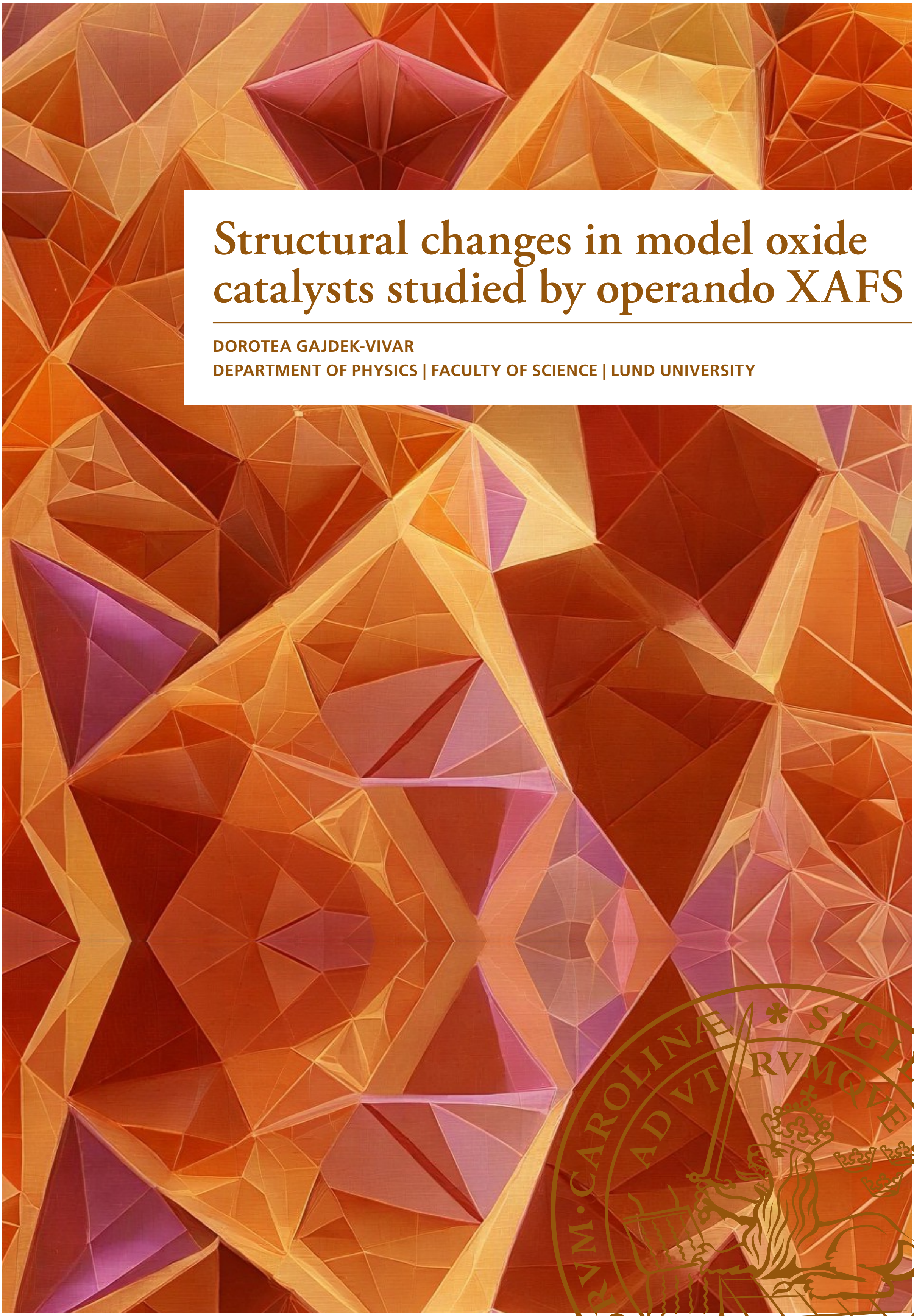

Structural changes in model oxide catalysts studied by operando XAFS

DOROTEA GAJDEK-VIVAR

DEPARTMENT OF PHYSICS | FACULTY OF SCIENCE | LUND UNIVERSITY

Structural changes in model oxide catalysts studied by operando XAFS

Structural changes in model oxide catalysts studied by operando XAFS

by Dorotea Gajdek-Vivar

LUND
UNIVERSITY

Thesis for the degree of Doctor of Philosophy
Thesis advisors: Docent Lindsay R. Merte, Prof. Edvin Lundgren,
Docent Sara Blomberg
Faculty opponent: Prof. Dr. Junfa Zhu

To be presented, with the permission of the Faculty of Science at Lund University, for public criticism in the Rydberg lecture Hall at the Department of Physics on Friday, the 11th of October 2024 at 13:15.

DOKUMENTDATABLAD enl SIS 61 41 21

Organization
LUND UNIVERSITY

Department of Physics
Box 118
SE–221 00 LUND
Sweden

Document name
DOCTORAL DISSERTATION

Date of disputation
2024-10-11

Sponsoring organization

Author(s)
Dorotea Gajdek-Vivar

Title and subtitle
Structural changes in model oxide catalysts studied by operando XAFS

Abstract

Bridging the pressure gap between surface science studies and industrial processes requires a combination of well-studied reactions, model systems as catalysts, and advanced techniques capable of detecting structural changes under realistic pressure conditions. Observations from such studies provide helpful insight into the present phases of the gas-surface boundary and transitions that happen during studied reactions.

This thesis utilizes *operando* X-ray absorption fine structure spectroscopy (XAFS) to study ultra-thin oxide films supported on single crystals under realistic reaction conditions. Grazing incidence geometry was used to probe only the topmost few layers of our surface. Ultra-thin CoO_x and FeO_x on Pt(111) were studied under ambient pressure exposure to CO and O_2, and CO oxidation conditions, where XAFS analysis revealed structural changes of the oxide films, depending on the gas atmosphere. Furthermore, operando time resolved measurement of FeO_x/Pt(111) indicate involvement of the trilayer phase in CO oxidation. The Sn/Pt surface alloys were studied during CO oxidation using GI-XANES, revealing the formation of Sn(II) oxides on the Sn/Pt surfaces under CO oxidation conditions. The found oxide qualitatively agrees with calculated spectra of previously studied tin surface oxides. Refle-XAFS was used to study chemical surface changes of industrial alloys and model electrodes in harsh electrochemical environments, without being limited to thin samples. NiMo powder catalysts were studied in transmission mode Quick-XAFS, which allowed for almost simultaneous data acquisition on both edges during in situ sulfidation reaction.

We have shown successful measurements in ambient pressure gas phase reaction conditions and harsh electrochemical conditions in liquid. Combining GI-XAFS with traditional surface science techniques such as low energy electron diffraction (LEED), scanning tunneling microscopy (STM), X-ray photoelectron spectroscopy (XPS), and auger electron spectroscopy (AES) is shown to be a very promising way begin to understand the structure of the catalyst before, during and after the chemical reaction.

Key words
thin films, heterogenous catalysis, model system, surface science, XAFS

Classification system and/or index terms (if any)

Supplementary bibliographical information

Language
English

ISSN and key title

ISBN
978-91-8104-131-6 (print)
978-91-8104-132-3 (electronic)

Recipient's notes

Number of pages
153

Price

Security classification

I, the undersigned, being the copyright owner of the abstract of the above-mentioned dissertation, hereby grant to all reference sources the permission to publish and disseminate the abstract of the above-mentioned dissertation.

Signature ____________________ Date 2024-08-26

Structural changes in model oxide catalysts studied by operando XAFS

by Dorotea Gajdek-Vivar

LUND UNIVERSITY

Cover illustration front: Impressionist adaptation of STM image of CoO thin film supported on Pt(111) generated by *Deep Dream Generator*.

Funding information: The research leading to this result was supported by the project CALIPSOplus under the Grant Agreement 730872 from the EU Framework Program for Research and Innovation HORIZON 2020. Funding for this research was provided by the Swedish Research Council (Grant nos. 2018-05374 and 2016-04162) and the Gyllenstierna Krapperup's Foundation. The DFT calculations were performed using computational resources provided by the Swedish National Infrastructure for Computing (SNIC) at the National Supercomputer Centre (NSC), Linköping University, and the High Performance Computing Center North (HPC2N), Umeå University.

Faculty of Science, Department of Physics

ISBN: 978-91-8104-131-6 (print)
ISBN: 978-91-8104-132-3 (electronic)

Printed in Sweden by Media-Tryck, Lund University, Lund 2024

NORDIC SWAN ECOLABEL
Printed matter
3041 0903

Media-Tryck is a Nordic Swan Ecolabel
certified provider of printed material.
Read more about our environmental
work at www.mediatryck.lu.se

MADE IN SWEDEN

To Adri,
who taught me how amazing one can be outside of their comfort zone.

Contents

List of publications

This thesis is based on the following publications, referred to by their Roman numerals:

I **Structural Changes in Monolayer Cobalt Oxides under Ambient Pressure CO and O_2 Studied by In Situ Grazing-Incidence X-ray Absorption Fine Structure Spectroscopy**

D. Gajdek, P. A. T. Olsson, S. Blomberg, J. Gustafson, P.-A. Carlsson, D. Haase, E. Lundgren, L. R. Merte

Journal of Physical Chemistry C, 126, 3411-3418 (2022)

I performed sample preparation and characterization by LEED, STM and AES, took part in the planning and performance of the XAFS experiments at the PETRA III synchrotron, performed the data analysis and prepared the first draft of the manuscript. I coordinated revision of the manuscript based on input from co-authors and reviewers.

II **Operando XANES Reveals the Chemical State of Iron-Oxide Monolayers During Low-Temperature CO Oxidation**

D. Gajdek, H. J. Wallander, G. Abbondanza, G. S. Harlow, J. Gustafson, S. Blomberg, P.-A. Carlsson, J. Just, E. Lundgren, L. R. Merte

Submitted

I performed sample preparation and characterization by LEED, STM and AES, took part in the planning and performance of the XAFS experiments at the MAX IV synchrotron, performed the data analysis and prepared the first draft of the manuscript. I coordinated revision of the manuscript based on input from co-authors.

III **Platinum-Tin surface alloys studied during O_2 exposure, and CO oxidation using grazing-incidence XANES**

H. J. Wallander, **D. Gajdek**, G. S. Harlow, J. Blomqvist, J. Just, M. Ciambezi, E. Lundgren, L. R. Merte

Submitted

I took part in the planning and performance of the XAFS experiments, contributed to the interpretation of the results and to revision of the manuscript.

IV **Probing the electrode-liquid interface using *operando* total-reflection X-ray absorption spectroscopy**

A. Grespi, A. Larsson, G. Abbondanza, J. Eidhagen, **D. Gajdek**, J. Manidi, A. Tayal, J. Pan, L. R. Merte, E. Lundgren

Surface Science 748 (2024)

I participated in the XAFS experiments and took part in the discussion of the results and of the manuscript.

V **Sulfidation of Supported Ni, Mo and NiMo Catalysts Studied by In Situ XAFS**

D. Gajdek, L. Idowu Ajakaiye Jensen, V. Briois, C. Hulteberg, L. R. Merte, S. Blomberg

Topics in Catalysis (2023)

I took part in the planning and performance of the XAFS experiments at the Soleil synchrotron, performed the data analysis and prepared the first draft of the manuscript. I coordinated revision of the manuscript based on input from co-authors and reviewers.

Related work

Publications not included in this thesis:

Structures of few-layer cobalt oxides on Pt(111)

D. Gajdek, H. J. Wallander, E. Lundgren, L. R. Merte

Manuscript

Dynamic Behavior of Tin at Platinum Surfaces during Catalytic CO Oxidation

H. J. Wallander, **D. Gajdek**, S. Albertin, G. S. Harlow, N., L. Buß, J. Krisponeit, J. I. Flege, J. Falta, E. Lundgren, L. R. Merte

ACS Catalysis, 13, 16158-16167 (2023)

The Oxygen Evolution Reaction Drives Passivity Breakdown for Ni–Cr–Mo Alloys

A. Larsson, A. Grespi, G. Abbondanza, J. Eidhagen, **D. Gajdek**, K. Simonov, X. Yue, U. Lienert, Z. Hegedüs, A. Jeromin, T. F. Keller, M. Scardamaglia, A. Shavorskiy, L. R. Merte, J. Pan, E. Lundgren

Advanced Materials, 35, 2304621 (2023)

Reduced Carbon Monoxide Saturation Coverage on Vicinal Palladium Surfaces: the Importance of the Adsorption Site

F. Garcia-Martinez, E. Dietze, F. Schiller, **D. Gajdek**, L. R. Merte, S. M. Gericke, J. Zetterberg, S. Albertin, E. Lundgren, J. E. Ortega

The Journal of Physical Chemistry Letters, 12, 39, 9508-9515 (2021)

Synthesis of Nano-engineered Catalysts Consisting of Co_3O_4 Nanoparticles Confined in Porous SiO_2

S. L. Zacho, **D. Gajdek**, J. Mielby, S. Kegnæs

Topics in Catalysis, 62, 621-627 (2019)

Atomic Layer Grown Zinc–Tin Oxide as an Alternative Buffer Layer for Cu_2ZnSnS_4-Based Thin Film Solar Cells: Influence of Absorber Surface Treatment on Buffer Layer Growth

N. M. Martin, T. Törndahl, M. Babucci, F. Larsson, K. Simonov, **D. Gajdek**, L. R. Merte, H. Rensmo, C. Platzer-Björkman

ACS Applied Energy Materials, 5, 11, 13971-13980 (2022)

List of Abbreviations

AES Auger Spectroscopy

AFM Atomic Force Microscopy

AP-XPS Ambient Pressure X-ray Photoelectron Spectroscopy

CUS Coordinated Unsaturated Sites

DFT Density Functional Theory

EC Electrochemical

EXAFS Extended X-ray Absorption Fine Structure

FCC Face Centered Cubic

GI-XAFS Grazing Incidence X-ray Absorption Fine Structure

h-BN hexagonal Boron Nitride

HDN Hydrodenitrogenation

HDO Hydrodeoxygenation

HDS Hydrodesulfurization

HP-STM High Pressure Scanning Tunneling Microscopy

LCA Linear Combination Analysis

LEED Low Energy Electron Diffraction

LEIS Low Energy Ion Scattering

MBE Molecular Beam Epitaxy

ML Monolayer

MvK Mars van Krevlen

PIPS Passivated Implanted Planar Silicon

RHEED Reflection High Energy Electron Diffraction

RT Room Temperature

QCM Quartz Crystal Microbalance

SIMS	Secondary Ion Mass Spectrometry
STM	Scanning Tunneling Microscopy
SXRD	Surface X-ray Diffraction
UHV	Ultra-High Vacuum
XAFS	X-ray Absorption Fine Structure
XANES	X-ray Absorption Near Edge Structure

Abstract

Bridging the pressure gap between surface science studies and industrial processes requires a combination of well-studied reactions, model systems as catalysts, and advanced techniques capable of detecting structural changes under realistic pressure conditions. Observations from such studies provide helpful insight into the present phases of the gas-surface boundary and transitions that happen during studied reactions.

This thesis utilizes *operando* X-ray absorption fine structure spectroscopy (XAFS) to study ultra-thin oxide films supported on single crystals under realistic reaction conditions. Grazing incidence geometry was used to probe only the topmost few layers of our surface. Ultra-thin CoO_x and FeO_x on Pt(111) were studied under ambient pressure exposure to CO and O_2, and CO oxidation conditions, where XAFS analysis revealed structural changes of the oxide films, depending on the gas atmosphere. Furthermore, the operando time-resolved measurements of FeO_x/Pt(111) indicate the involvement of the trilayer phase in CO oxidation. The Sn/Pt surface alloys were studied during CO oxidation using GI-XANES, revealing the formation of Sn(II) oxides on the Sn/Pt surfaces under CO oxidation conditions. The found oxide qualitatively agrees with the calculated spectra of previously studied tin surface oxides. Refle-XAFS was used to study chemical surface changes of industrial alloys and model electrodes in harsh electrochemical environments, without being limited to thin samples. NiMo powder catalysts were investigated in transmission mode Quick-XAFS, allowing almost simultaneous data acquisition on both edges during the in situ sulfidation reaction.

We have shown successful measurements in ambient pressure gas phase reaction conditions and harsh electrochemical conditions in liquid. Combining GI-XAFS with traditional surface science techniques such as low energy electron diffraction (LEED), scanning tunneling microscopy (STM), X-ray photoelectron spectroscopy (XPS), and auger electron spectroscopy (AES) is shown to be a very promising way begin to understand the structure of the catalyst before, during and after the chemical reaction.

Popular Summary in English

Considering the steep increase of the global electricity demand and oversaturation of the electricity grid, the use of hydrogen as an energy carrier, and fuel cells as means to produce electrical energy from said hydrogen would enable faster electrification with renewable resources. One of the key processes for the production of clean hydrogen fuel for the polymer electrolyte membrane fuel cell (PEFC) is the preferential oxidation of carbon monoxide in excess hydrogen (PROX). This is one of the many reason why oxidation of toxic carbon monoxide (CO) to carbon dioxide (CO_2) is a crucially important chemical process today.

Platinum is the most widely used and active catalyst for CO oxidation. However, even though it is the most active, platinum has its own set of problems. The most obvious problem is the price of platinum itself, followed by the availability, cost, and complexity of platinum mining. On a more scientific side, platinum catalysts are active in CO oxidation only at high temperatures, which means they are energetically expensive. Platinum gets very easily poisoned by CO, which significantly reduces the activity of the catalyst.

One of the goals of many worldwide is to find a cheaper catalyst that is readily available in nature and has high activity towards CO oxidation in mild conditions, which makes it automatically greener than a platinum catalyst. Since catalysts are highly complex systems, mainly when employed in industrial processes, scientists developed a simpler concept named *model catalyst*. Model catalysts mimic realistic industrial catalysts and, therefore, allow for an in-depth understanding of the atomic level of what is happening on the surface during a chemical reaction. Simply put, we want to know what atoms do on, and above the surface as the reaction occurs.

CO oxidation is a heterogeneous catalytic reaction meaning the reactant and the catalyst are in different phases. Specifically, these phases are a solid material (catalyst) and a gas (reactant). To shed light on the processes taking place during such chemical reaction, we have to measure as the reaction occurs while the catalyst is "working." Such measurement is called an *operando* measurement for which we require *operando* techniques. Since we want to understand how a new catalyst can be used in real life, we want to study changes occurring at the surface under realistic conditions, meaning high pressures and temperatures. Finally, we want to understand how the catalyst changes during the reaction and what is its lifetime. For that, we need to perform time-resolved measurements.

This thesis primarily aims to understand the processes occurring during CO oxidation at realistic conditions over several materials that were shown to be promising catalysts for low-temperature CO oxidation. We have shown that it is possible to adapt non-traditional X-ray techniques for surface science studies and employ them in a time-resolved *operando* set up to gather chemical and structural information about our surfaces during realistic conditions. Furthermore, we have shown that such a technique can also be used in liquid environments, such as electrochemical cells, which opens up the doors for more exciting science, hopefully driving catalytic innovations toward greener materials in processes in gas environments and liquid ones.

Populärvetenskaplig sammanfattning på svenska

Med kraftigt ökad efterfrågan på el och överbelastningen av elnätet, skulle användningen av väte som energibärare, och bränsleceller att producera elektrisk energi från vätet möjliggöra snabbare elektrifiering med förnybara resurser. En av nyckelprocesserna för framställning av rent vätebränsle för polymerelektrolytmembranbränslecellen (PEFC) är är att kunna oxidera spår av kolmonoxid i ett vätgasflöde (PROX). Detta gör CO-oxidation, där giftig kolmonoxid (CO) oxideras med syre till koldioxid (CO_2), till en mycket viktig kemisk process i dagens samhälle.

Platina är den mest använda och mest aktiva katalysatorn för CO-oxidation. Men trots att den är den mest aktiva katalysatorn, har platina sina egna problem. Det mest uppenbara problemet är priset på själva platinan, följt av tillgängligheten, kostnaden och komplexiteten för platinabrytning. På en mer vetenskaplig nivå är platinakatalysatorer aktiva i CO-oxidation endast vid höga temperaturer, vilket innebär att de är dyra i drift. Platina blir mycket lätt blockerad av CO, vilket minskar katalysatorns aktivitet avsevärt.

Ett av målen är att hitta en billigare katalysator som är lättillgänglig i naturen och har hög aktivitet mot CO-oxidation under milda förhållanden, vilket automatiskt skulle göra den grönare än en platinakatalysator. Eftersom katalysatorer är mycket komplexa system, främst när de används i industriella processer, utvecklade forskare en enklare model som kallas *modellkatalysator*. Modellkatalysatorer liknar realistiska industriella katalysatorer och möjliggör därför en djupare förståelse av vad som händer på ytan under en kemisk reaktion på atomnivå. Enkelt uttryckt vill vi veta vad som händer med atomerna på och ovanför ytan när reaktionen sker.

CO-oxidation är en heterogen katalytisk reaktion vilket betyder att reaktanten och katalysatorn är i olika faser. Specifikt är dessa faser ett fast material (katalysator) och en gas (reaktant). För att förstå de processer som äger rum under en sådan kemisk reaktion måste vi mäta när reaktionen sker medan katalysatorn ärbetar". En sådan mätning kallas en *operando*-mätning för vilken vi kräver *operando*-tekniker. Eftersom vi vill förstå hur en ny katalysator kan användas i verkligheten, vill vi studera förändringar som sker på ytan under realistiska förhållanden, det vill säga höga tryck och temperaturer. Slutligen vill vi förstå hur katalysatorn förändras under reaktionen och vad dess livslängd är. För att göra det behöver vi utföra tidsupplösta mätningar.

Denna avhandling syftar främst till att förstå de processer som sker under CO-oxidation vid realistiska förhållanden över flera material som visat sig vara lovande katalysatorer för CO oxidation vid låg temperatur. Vi har visat att det är möjligt att anpassa icke-traditionella röntgentekniker för ytvetenskapliga studier och använda dem i en tidsupplöst *operando* uppsättning för att samla kemisk och strukturell information om våra ytor under realistiska förhållanden. Dessutom har vi visat att en sådan teknik också kan användas i vätska, till exempel elektrokemiska celler, vilket öppnar dörren för mer spännande vetenskapliga studier.

Acknowledgements

Some say that PhD journey is a lonely one. I can safely confirm that was not true in my case. Over the past five and a half years, I had a chance to learn, share knowledge and have a lot of fun with a fantastic group of people. They all took part in shaping me into the person I am today, and I thank them all for that.

To begin with, I would like to thank my main supervisor **Lindsay R. Merte**. You introduced me to the world of synchrotrons and surface science, you were always ready to happily share your detailed knowledge with me, for which I will forever be thankful for. You never hesitated in taking time for discussions and any help one might need. Thank you for all the end-of-summer BBQs and for making all your PhD students feel so welcome and accepted.

Edvin Lundgren was my second supervisor. Thank you, Edvin, for all the discussions in Obelix, for all the interest in my samples and results. Thank you for organizing many workshops and a winter school in Italy. Attending schools and conferences with you is a special experience - a perfect mix of learning, networking and fun.

To my co-supervisor, **Sara Blomberg**, I thank for including me in her NiMo project and all the learnings that came out of every discussion we had. Thank you for many fun drives to Hamburg and back, to many successful beamtimes shared and for always making sure we have enough candy to last through those long night shifts.

A fellow PhD student, and a friend, with whom I worked most closely with is **Harald J. Wallander**. Thank you, Harald, for sharing this experience with me, everything from learning how to operate and maintain Skalman, to beamtimes, summer and winter schools, and conferences. Thank you for being so kind to people, and so open to share insanely interesting knowledge about sailing, plants and Swedish nature parks.

A big thank you goes to everyone at the Division of Synchrotron Radiation at Lund University. Thank you for being a part of my journey and for making those confusing hallways feel familiar. Specially, I would like to thank **Estephania Lira**, for her help with STM, and everything Obelix related, and for her friendly approach in both professional and personal matters. I have had a chance to meet many PhD students at the division, amongst which I would like to mention **Stefano Albertin** - thank you for being my Obelix go-to, for board game nights and long discussions about anything and everything. **Andrea Grespi** and **Alfred Larsson**, thank you both for including me in your electrochemistry world, and thank you for fun times in Hamburg, both inside and outside of the synchrotron.

Lisa Rämisch and **Sabrina Gericke** from Combustion Physics, it was incredibly nice having you on this journey with me. Thank you for all the laughs and new experiences during the SURFCAT summer school, and for our short but productive time together in Obelix. **Johan Zetterberg**, thank you for hiring Lisa and Sabrina, for interesting discussions, and for always being open to help and advise.

The MTM Department at Malmö University was a place where I spent a lot of my time over these years. Thank you, **Madeleine Burheim**, **Asimina Papoulia**, and **Samuele Sottile** for being so welcoming and kind in the beginning of my PhD journey. To my amazing office mates - **Sana Khayyamifar**, **Shilpa Bijavara Seshashayana**, **Andrea Morales Rodríguez**, **Mattias Tidefelt**, **Grzegorz Sadowski**, **Miguel Kofoed**, **Pedro Moya**, **Indrajeet Tambe**, and Madeleine and Harald, without you, this journey would have been very lonely. I will always remember our office as a friendly, fun place filled with laughter, ranting, scientific discussions and never ending candy resources. Thank you for all the board game sessions, ice cream breaks and after works. There have been many administrators and seniors involved in my journey, they deserve a mention too. Thank you **Andreas Krause** for always being there to help with the lab and teaching, thank you for joining our board games and for always making us all laugh. Thank you, **Christina Bjerkén** for sharing your passion and knowledge about sustainability, it was a pleasure to learn from you. **Pär Olsson**, thank you for the help with the DFT and for always being ready to discuss the results. **Milan Burke**, thank you for being such a joyful person, it was a pleasure to hang out with you and share experiences. **Peter Falkman**, thank you for being such a helping hand around our lab, and for never hesitating to share your knowledge with me. Finally, a big thank you goes to **Katja Frid** and **Mats Persson** for making sure our department runs smoothly, and everyone has a pleasant working experience.

It would be very hard to do our work without synchrotrons. Therefore, a lot of gratitude goes to everyone who has helped make our experiments run over the past years. From Balder beamline at MAX IV, a big thank you goes to **Justus Just** and **Mahesh Ramakrishnan** for all the sleepless nights and shared excitement for our results. From P64 beamline at PETRA III, I would like to thank **Wolfgang Caliebe** for his support during our time there. **Francesco Carlà** and **Hadeel Hussain** from I07 at Diamond, thank you for the time and dedication during our beamtime. Finally, thank you **Valerie Briois** from

ROCK beamline at SOLEIL for all the knowledge shared about our results, and about the beamline itself.

It goes without saying that non of these would be possible without my "village". To some of my oldest and closest friends, **Dora S.**, **Amadea**, **Sandra**, **Sarah** and **Sid** - thank you for being there for me since the beginning. I would have not been the same person as I am now without each and every one of you contributing to it in their own special way.

Hvala, **mama Sanja** i **tata Damir**, for always encouraging me to follow my dreams, even if that meant moving so far away. Your unconditional love and support are the reason I am here today. Hvala, **Luka**, my baby brother, for being such fun person to grow up with. I love seeing how you grow and what an amazing person you are. Never change. Gracias to my parents in law, **Emilio** and **Dolores**, for welcoming me to your family and being such great cheerleaders on this journey.

Finally, the biggest, mushiest thank you goes to my best friend, my biggest supporter, my ride-or-die and a father to the most amazing little girl. Thank you, **Adrian**, for being you. Kalea and I are incredibly happy to have you.

Structural changes in model oxide catalysts studied by operando XAFS

Doing something that nobody else has done before is actually quite hard.
— Dr. Ruben Rausing

Chapter 1

Introduction

Catalysts and catalysis have been an essential part of everyday life since the beginning of human history. The first mention of a substance that sped up the reaction was in 1552 by Valerius Cordus, who used sulfuric acid to catalyze the conversion of alcohol to ether.[1] Later, Johan Wolfgang Döbereiner found that when starch is dissolved in water, it ferments into alcohol.[2] Although these processes have been observed and described in literature many years before, it took until 1835 for this phenomenon to have a name. Jöns Jakob Berzelius named the process *catalysis*. The term was derived from the Greek word *kata* meaning "down," and the Greek word *lyein*, meaning "loosen".[3]

Out of many blooming discoveries that followed the ones already mentioned, I would like to focus on Paul Sabatier and Jean-Baptiste Senderens, who discovered catalytic hydrogenation which gave Sabatier a Nobel Prize in Chemistry in 1912.[3] Hydrogenation of inorganic molecules (CO and CO_2) to hydrocarbons has led to some of the most critical industrial processes: the Haber-Bosch ammonia synthesis, the Fischer-Tropsch and methanation reactions, all petrochemical processes involving hydrogenation/dehydrogenation, etc.[4,5] The research done by Sabatier and his students led to the discovery of nickel and platinum group metals, both alone and supported, as incredibly active catalysts, especially for hydrogenation reactions.

As we can see, catalysts are playing a crucial role in the development of the world. Our society is battling an energy crisis, which means that the need to reduce the carbon footprint is more significant than ever. Catalysts play a considerable role in this battle since every industrial process includes a catalyst. This leads to an ever-growing desire to make new and better catalysts. In order to make new, better, and greener catalysts, one must first understand the catalyst material to its core. In the past, catalyst materials were developed by employing trial and error methods, which was very time and resource consuming. The introduction of the "surface science approach" by Irving Langmuir in 1922[6] provided a new pathway for studying elementary processes underlying chemical reactions at surfaces. The surface science approach allows scientists to gather a fundamental understanding of catalysis, which is then used to design catalysts with specific properties perfectly tailored for each reaction they catalyze.[7] Langmuir suggested that model systems, mainly well-characterized single crystal surfaces, can be used in a highly controlled environments, such as ultrahigh vacuum systems (UHV), to study mentioned elementary processes. This approach is widely used nowadays on various complex systems such as heterogeneous materials, nanoparticles, alloys, and oversimplified model systems in UHV and in complex conditions: high pressures, high temperatures, liquid environments, reaction conditions, etc.

The birth of new scientific ideas had to be followed by technological innovations. The equipment availability during Langmuir's time made it quite hard to achieve UHV conditions, which, of course, limited the possibilities to study materials in depth. However, the development of stainless steel vacuum hardware and vacuum pumps in 1960 resulted in a rapid development of UHV technology, which led to a fast growth of the field of surface science.[8,9] In only 10 years after UHV development, surface analysis techniques grew from non to more than twenty.[8] It is still growing today with new technological developments and research questions.

The importance of the surface science approach to the scientific community can best be shown by the extensive amount of Nobel Prizes awarded in relation to it. In 1981[10], Kai Siegbahn was awarded a Nobel Prize in Physics for "his contribution to the development of high-resolution electron spectroscopy," making X-ray spectroscopy suitable for surface science studies. In 1986[11], Gerd Binnig and Heinrich Rohrer were awarded a Nobel Prize in Physics "for their design of scanning tunneling microscope", which is today one of the most used imaging techniques in surface science studies. We know today that experimental and theoretical research complement each other and are necessary, especially in surface science studies. Thanks to Walter Kohn "for his development of the density-functional theory" and John A. Pople "for his development of computational methods in quantum chemistry" (Nobel Prize in Chemistry in 1998[12]), we can combine experiments and theory in our research and drive new ideas further than ever before. Since in this work, and in the majority of surface science research, we study chemical reactions on surfaces, it is mandatory to mention

Gerhard Ertl, who was awarded the Nobel Prize in Chemistry in 2007[13] "for his studies of chemical processes on solid surfaces".

As previously mentioned, surface science is widely used to study catalyst materials in detail. However, the complexity of industrial catalysts makes it quite hard to perform fundamental surface science studies on them. A common approach in surface science to combat the complexity of these systems and technological limitations is to use *model systems*. Model systems are an over-simplified version of complex industrial catalysts. They usually consist of a metal single crystal surface and an active layer supported on the single crystal. There are many other variations of model systems, depending on the research question at hand, such as nanoparticles of active material dispersed on an inactive support. Model systems are excellent for studying interactions between the active material and the support, and for studying reactions on the surface in before mentioned UHV or low pressure conditions. As one can notice, these mentioned conditions are far away from the realistic reaction conditions that industrial catalysts are exposed to. The discrepancy between real life conditions and research conditions is called *materials and pressure gap*. To bridge the materials gap, surface scientists have worked tirelessly over the past years to develop more complex model systems such as polycrystalline samples and size-controlled nanoparticles. On the other hand, instrumental development played a crucial role in bridging the pressure gap. Today, we can achieve higher pressures in experimental setups while still observing reactions on the surfaces of model systems, therefore slowly bridging materials and pressure gaps.

1 Bridging the pressure gap with X-ray absorption fine structure spectroscopy

As discussed previously, fundamental surface science experiments were limited to UHV conditions. On the one hand, UHV conditions are highly beneficial since they allow for detailed control of the sample surface and experimental conditions, which is essential when studying fundamental properties of a material. On the other hand, UHV conditions prevent experiments at realistic temperature and pressure conditions. For instance, under UHV conditions, we may not be able to observe certain reactions that occur at higher pressures, such as the adsorption of gas molecules on a surface. This leads to a lack of understanding of reaction mechanisms on material surfaces.

In UHV, the low density of particles in the vacuum chamber allows for an atomically clean surface to be prepared and maintained for the duration of the experiment. Electron and ion-based characterization techniques operated under UHV conditions allow for studies without gas phase interference in the scattering events, which is quite useful to study fundamental properties of materials. Some of the surface science techniques traditionally used under UHV conditions are low energy electron diffraction (LEED), reflection high energy electron diffraction (RHEED), scanning tunneling microscopy (STM), X-ray photoelectron spectroscopy (XPS), near edge X-ray absorption fine structure (NEXAFS), surface X-ray diffraction (SXRD), secondary ion mass spectrometry (SIMS) and low energy ion scattering (LEIS). Since these techniques are traditionally used in UHV conditions, they provide information about the sample before and after a reaction, meaning they are used for ex-situ experiments. To study a sample under high temperature and pressure conditions, i.e. realistic reaction conditions and during the reaction itself, i.e. operando, experiments should be performed outside of the UHV regime. In order to learn about structural changes of materials during a chemical reaction, as well as reaction mechanisms on the surface of those materials, measurements at high pressures and temperatures, and in situ and operando are necessary. Technological developments in recent years allow for some UHV techniques to operate at elevated pressures, bridging the pressure gap and allowing in situ studies of catalysts and their interaction with reactants, shedding light on reaction mechanisms. Some of the UHV techniques adapted to elevated pressures are ambient pressure X-ray photoelectron spectroscopy[14] (AP-XPS) and high-pressure scanning tunneling microscopy[15] (HP-STM).

AP-XPS, a technique widely used for characterizing the chemical states of materials in gases and liquids, operates in the mbar to bar pressure ranges. While it is highly versatile and capable of providing information about almost all elements at the sample surface and in the gas or liquid phase, the information about specific species is usually derived from the binding energy alone, providing only a nominal oxidation state. Understanding the pressure gradient near the sample surface, a direct result of the photoelectron extraction mechanism, is crucial as it imposes restrictions on the reaction conditions and the possible reaction kinetics that can be probed. To complement possible findings using AP-XPS and allow for measurements under a wider range of conditions, and to probe reaction kinetics, we intended to use X-ray absorption fine structure spectroscopy (XAFS) under in situ and operando regimes. XAFS is a hard X-ray technique, meaning it can be used at high pressures, higher than pressures allowed for AP-XPS. This quality of XAFS allows for bridging the pressure gap by studying model catalysts under realistic reaction conditions. Since XAFS allows for measurements at harsh pressure and temperature conditions, while providing high signal-to-noise ration, it is possible to gain insight into the reaction kinetics.

XAFS is a potent technique broadly applied to characterize in situ materials. Measurements of the fine structure near the absorption edge (XANES - X-ray near edge absorption fine structure spectroscopy) of an element provide a chemical fingerprint, allowing for the identification of phases present, while the analysis of the fine structure above the edge (EXAFS - extended X-ray absorption fine structure spectroscopy) provides information of the local structure and bonds.[16–18] Traditionally, XAFS is used for studying bulk materials due to hard X-rays' considerably high sampling depth, meaning that adaptation is needed to serve as a surface science technique. Implementing grazing incidence geometry and fluorescence detection allows for studying species exclusively found at the material's surface. This geometry provides sufficiently high signal-to-noise ratios, which enable the characterization of structural changes and local bonding environments for sub-monolayer oxide films serving as model systems for catalytic reactions.

This work, utilizing grazing incidence XAFS (GI-XAFS), has successfully bridged the pressure gap on various catalytic systems. In **Paper I**, we focus on in situ observations of structural changes in monolayer cobalt oxides under ambient pressure CO and O_2 conditions. The practicality of this study lies in its ability to identify the Co phases present and their transformations under oxidizing and reducing conditions. This was achieved by measuring GI-XAFS during surface exposure to gases at elevated temperatures. This study, to our knowledge, was the first ever attempt to study monolayer oxide model systems using GI-XAFS. The results demonstrate the power of this technique in probing the structures of well-defined oxide monolayers under realistic catalytic conditions but also highlight its potential for real-world applications. The learning from the fist attempt allowed us to improve our experimental setup, sample transfer and detectors used, with the goal to achieve higher signal-to-noise ratio compare to the first attempt, and to perform faster time resolved measurements. This was done in **Paper II**, where we further utilized this technique in the operando regime, studying the chemical state of iron during low-temperature CO oxidation by FeO_x/Pt(111). This was achieved by performing measurements in time resolved manner, which contributed to understanding the mechanism behind CO oxidation over thin iron oxide films supported on platinum single crystal. The results highlight the unique properties of monolayer FeO and the importance of the Pt support in CO oxidation. The next step was to utilize GI-XAFS to understand the dynamic behavior of Pt/Sn surface alloys under ambient pressure CO oxidation conditions, presented in **Paper III**. This means we extended the use of GI-XAFS over ultra-thin oxides to much higher photon energies, which presents its own challenges. However, this study can be seen as the first step towards successful studying of PtSn fuel cell catalysts since results shed light on the reactivity of this highly promising catalyst.

One of the challenges when studying electrochemical (EC) processes, where chemical changes of interest take place at the surface of the electrode and at the electrode-electrolyte interface, is the limitation of the techniques to be used only ex-situ, due to the need for surface sensitivity. In **Paper IV**, we used operando X-ray absorption spectroscopy in total external reflection geometry (Refle-XAFS) with a simple and versatile EC flow cell. This study showed that Refle-XAFS can be used in harsh electrochemical environments to study chemical changes of industrial alloys and model electrodes.

To gain a better understanding of structural changes in a complex industrial catalyst during a chemical reaction, it would be desirable to study multiple elements almost simultaneously. This is made possible using Quick-EXAFS at the ROCK beamline at SOLEIL synchrotron in France, which allows for fast alternation between two absorption edges. In **Paper V**, we have used Quick-EXAFS to study in-situ sulfidation of Ni- and Mo- based catalysts by following the species' oxidation state during the process. The edge-jump method and its high temporal resolution made it possible to follow the transition from the oxide precursor to the active sulfide phase while characterizing both the Mo and the promoter metal. The light is also shed on the importance of the oxide support in the sulfidation processes.

Chapter 2

Catalysis and Model systems

Since this thesis's work is focused on catalysts and catalytic reactions, this chapter will give a brief introduction to catalysis, how catalysts facilitate chemical reactions, and model systems as catalysts. Finally, an overview of research done on three model systems studied in this thesis (CoO_x/Pt(111), FeO_x/Pt(111), and Pt/Sn alloys and oxides) in CO oxidation is given, as well as an overview of the research done on an industrial system studied in this work, the NiMo-based catalyst.

1 Catalysis

A *catalyst* is a substance which speeds up a chemical reaction, or causes milder temperature and/or pressure conditions needed to start a reaction, without being consumed itself, in a phenomena known as *catalysis.*[19]

There are two types of catalysis: homogeneous and heterogeneous catalysis. In homogeneous catalysis, the catalyst is in the same phase as the reactants. Some examples of homogeneous catalysis are hydrolysis of esters by mineral acids or alkalis, acid-catalyzed esterification and oxidation of ethylene to acetaldehyde in the presence of palladium (II) chloride and copper (II) chloride as the catalyst. In heterogeneous catalysis, the catalyst and the reactants are in different phases. Most often, the catalyst is in a solid phase while the reactants are either in a gas or liquid phase. One of the most famous heterogeneous catalytic reactions is the Haber-Bosch process for production on ammonia. Here, the atmospheric nitrogen reacts with hydrogen, and is converted to ammonia using an iron metal catalyst under high pressures and temperatures. Another very well known heterogeneous catalytic reaction is the CO oxidation, where poisonous carbon monoxide reacts with oxygen to carbon dioxide, using platinum metals as catalysts.

When talking about a chemical reaction, one must think about *thermodynamics* and *kinetics* of the reaction. Chemical thermodynamics dictates the direction of a reaction and a "$\rightleftarrows$" symbol is used to indicate a thermodynamic equilibrium of a reaction according to *Le Chatelier's principle.*[20] This means that if a system at an equilibrium state undergoes concentration, pressure, volume or temperature changes, the system will readjust itself to partially counter the effect of the said change, resulting in a new thermodynamic equilibrium. A thermodynamic equilibrium for a given pressure and temperature will have smaller Gibbs free energy, ΔG than that of any other state with the same pressure and temperature. In the example of CO oxidation, the reaction would be written as:

$$CO + \frac{1}{2}O_2 \rightleftarrows CO_2 \tag{2.1}$$

Reaction kinetics gives information about the rate at which the reaction takes place, reaction's mechanism and transition states. Potential energy diagram is typically used to illustrate a reaction path and it is an excellent representation of the work a catalyst does in a reaction. Potential energy diagram for CO oxidation without a catalyst and over a Pt(111) catalyst surface is shown in Figure 2.1. The red line represents the energy needed to produce CO_2 without a catalyst, which is quite high, making the reaction very slow. With the introduction of a catalyst into the reaction system, a new reaction path is created between the reactants and the product, allowing for the reaction to proceed at a speed several orders of magnitude higher than without a catalyst. Furthermore, it can be seen that the Gibbs free energy, ΔG stays unchanged if the catalyst is used since the catalyst does not affect the thermodynamic equilibrium, only reaction kinetics.

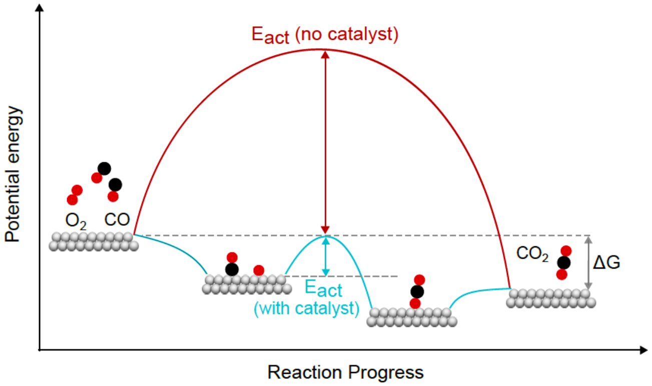

Figure 2.1: Schematic representation of a potential energy diagram for CO oxidation without a catalyst (red line) and over Pt(111) catalyst surface (blue line) adapted from reference.[19]

1.1 Heterogeneous catalysis

As mentioned, reactants and catalysts are in different phases in heterogeneous catalysis. The catalyst is always a solid material, while the reactants are either in gas or liquid phase. In heterogeneous catalysis, the reaction usually takes place at the surface of a material, which means that a high surface area of a catalytic material is desirable.

A reaction mechanism is a sequence of elementary reactions which build an overall chemical reaction.[21] A commonly invoked reaction mechanism is called the Langmuir-Hinshelwood mechanism, which can be described by the following steps: adsorption, diffusion, dissociation, recombination, and desorption. **Adsorption.** There are two kinds of adsorption, physisorption and chemisorption, depending on the strength of the bonds between the adsorbate and the surface. Weaker interactions, such as Van der Waals forces, result in physisorption and typically this type of adsorption does not include a chemical reaction. Chemisorption occurs when a chemical bond forms between an adsorbate and the surface; hence, a chemical reaction occurs on the surface of a material. The illustration of a potential energy diagram for physisorption and chemisorption is shown in Figure 2.2a. After a molecule has been adsorbed on the surface, it will potentially dissociate into atoms or smaller molecules and diffuse around the surface. **Diffusion.** Surface diffusion is the movement of atoms and molecules on a solid surface between available absorption sites. It is usually thermally driven, meaning the diffusion rate increases with temperature. Figure 2.2b illustrates a potential energy diagram for a diffusion process of an adsorbate between available absorption sites on a surface. **Recombination** Recombination is a process in which the adsorbed molecules diffuse on the surface until they react with each other, forming a product. The final step is the desorption of a product from a catalyst surface. **Desorption.** Desorption is a process opposite of adsorption. This process removes freshly formed products from a catalyst surface and frees up space for new adsorbates on the surface.

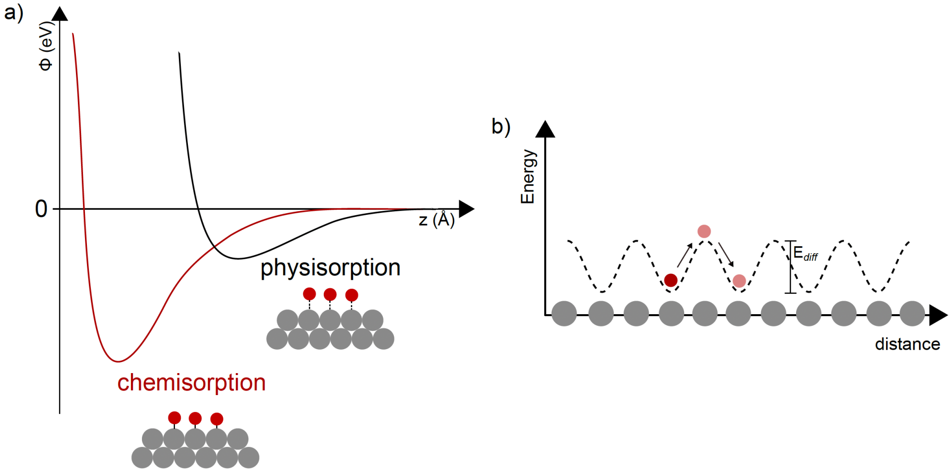

Figure 2.2: a) Illustration of a one-dimensional potential energy diagram for physisorption and chemisorption. b) Illustration of a potential energy diagram for a diffusion process of an adsorbate between available adsorption sites on a surface.

There are three known reaction mechanisms in heterogeneous catalysis: the Langmuir-Hinshelwood, the Eley-Rideal, and the Mars-van Krevelen type reaction mechanism. As already mentioned, in the Langmuir-Hinshelwood type mechanism, both reactants are first chemisorbed on the surface of the catalyst where the reaction will take place, and finally, the product will desorb from the surface back into the gas phase. For example, when CO oxidation is catalyzed over Pt(111) metallic surface[22], it follows this type of mechanism. In the Eley-Rideal type mechanism, one reactant is chemisorbed on the surface of a catalyst while the other reactant is in the gas phase. Finally, in the Mars-van Krevelen type mechanism, the reactants adsorb on the surface of an oxide catalyst, where they react with oxygen from the surface layer. It has been reported that CO oxidation over RuO_2[23] and PdO[24] follows the Mars-van Krevelen type mechanism. Schematic representations of all three reaction mechanisms in heterogeneous catalysis are shown in Figure 2.3.

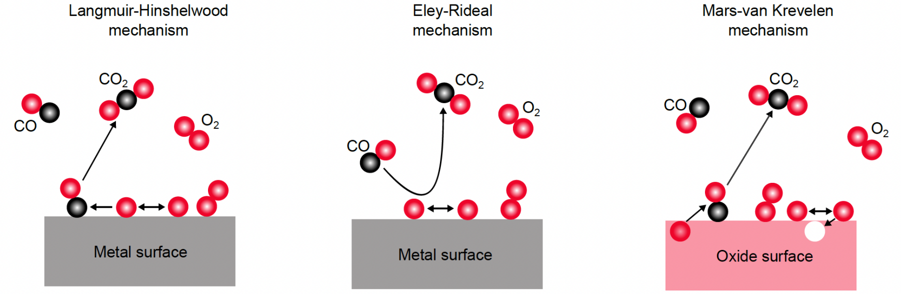

Figure 2.3: Schematic representations of all three reaction mechanisms in heterogeneous catalysis: a) Langmuir-Hinshelwood type mechanism, b) Eley-Rideal type mechanism and c) Mars-van Krevelen type mechanism.

2 Model catalysts

Industrial catalysts are highly complex systems with many facets and interfaces in one material. In this work, we aim to study fundamental processes on simplified materials. These materials are called *model catalysts*, and they intend to mimic certain facets of complex industrial catalysts. Model catalysts studied in this thesis are ultra-thin oxides supported on Pt(111) single crystals.

Single crystals are materials in which the crystal lattice is made of uninterrupted repetition of the unit cell in all three dimensions.[25] The surface of a single crystal corresponds to a specific crystal plane, which depends on the orientation in which the bulk crystal is truncated. Different orientations within a crystal are distinguished by the so-called Miller indices - *h, k, l*. In surface science, Miller indices are used to identify the lattice plane along which a crystal is cut to obtain a specific *(hkl)* surface. When an FCC metal is cut in a way that the surface plane intersects the lattice vectors ($\overrightarrow{a_1}$, $\overrightarrow{a_2}$, $\overrightarrow{a_3}$) at the same value, a (111) surface is exposed. Figure 2.4 a and b, show an example of how to obtain a low index surface with (111) orientation, and an illustration of a platinum (111) surface plane, respectively.

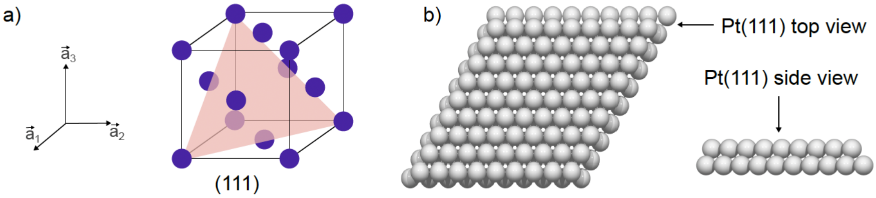

Figure 2.4: Illustration of a) (111) low index crystal planes of FCC unit cell, b) top and side view of platinum (111)surface plane.

Oxides play important roles in chemical processes, which makes them an interesting substances to study. Surface science studies of well-defined oxide films are becoming popular, since they provide a pathway to study a complex role of an oxide in a chemical reaction, in a simplified manner. Supported oxides can provide knowledge about the oxide itself and its role in a chemical reaction, as well as knowledge about the interactions between the oxide and the metal. Supported oxides can be found in several forms as model catalysts, such as metal nanoparticles on oxide supports, ultra-thin oxide films supported on metal single crystals, and native oxide films on metals. In this thesis, we focus on ultra-thin oxide films supported on metal single crystals as they are promising model systems to study oxides as surface materials in catalytic reactions. By placing the oxide layer on top of a metal surface, an approach is created where interfacial sites can be controlled, reaction mechanisms on the oxide and/or the metal-oxide interface can be studied, and stability, activity and selectivity of the catalytically active material can be studied and improved.[26]

Ultra-thin oxide films have been extensively grown on Pt(111) single crystals in the past years. The (111) surface of platinum is a widely used substrate in fundamental catalytic studies mainly due to its close packed structure, which provides high stability in possible adsorption-induced surface reconstructions.[27]

2.1 CoO_x on Pt(111)

Many studies have shown an increased catalytic activity of oxide-metal mixed catalysts due to the role of the oxide-metal interface.[28–38] A combination of platinum (Pt) metal and cobalt oxides received quite a bit of attention due to its high catalytic activity towards low temperature CO oxidation.[39,40] The main advantage of cobalt oxides, when combined with platinum, is blocking the CO poisoning of the surface, which is what happens on bare platinum catalysts. However, the deactivation of the cobalt oxide catalysts can take place due to water dissociation to form hydroxyls.[41] The reaction pathway of CO oxidation over cobalt oxide-platinum catalysts will depend on many parameters, such as the sample temperature, CO/O_2 ratio, structure of the catalyst, etc.[42] Therefore, it is important to mention that cobalt oxide-platinum catalysts come in many shapes and forms, such as Pt nanoparticles encapsulated in cobalt oxides,[34,43] and atomically coupled Pt nanoparticles with single-crystal CoO nanorods.[44]

Since the addition of cobalt oxides to platinum shows great potential as catalysts for CO oxidation, it is essential to study and understand the mechanisms underlying this activity. For this purpose, using model systems and a surface science approach is inevitable. The model system for this purpose is a sub-monolayer cobalt oxide thin film supported on a platinum (111) surface. In this system, cobalt oxide is the surface material, completely exposed to the reaction conditions. This configuration of a model catalyst allows for studies of structural changes of the oxide, role of the oxide in the reaction, and role of the oxide-metal interface in the enhanced activity of the catalyst.

Sub-monolayer cobalt oxide thin films are grown on Pt(111) by reactive deposition of metallic Co in an oxygen atmosphere, resulting in hexagonal bilayer films with lattice spacing of 3.13Å and buckling of Co atoms (shown in Figure 2.5, left). CoO thin films exhibit structural changes when exposed to reducing and oxidizing conditions in high vacuum. Specifically, the CoO bilayer transforms into CoO_2 trilayer upon oxygen exposure[45,46], shown in Figure 2.5, right. Extensive studies on cobalt oxide thin films on platinum support in CO oxidation give insight into the mechanisms taking place during the reaction. Fester et al.[46] performed an ex-situ study on CoO_x/Pt(111) in CO oxidation. STM and XPS studies revealed that bilayer CoO structures facilitate CO oxidation at lower temperatures when compared to fully oxidized CoO_2 trilayers. Furthermore, Kersell et al.[41] performed an operando investigation on such model systems at room temperature (RT) and in the mTorr pressure range. They used AP-XPS as the main technique in their research, combined with HP-STM and density functional theory (DFT) calculations. They found partially oxidized CoO surfaces to be highly active for CO oxidation at RT, while surfaces lacking O vacancies had significantly lower activity towards CO_2 formation. Furthermore, they observed poisoning of the catalyst by carbonate formation when edges of CoO islands were exposed, thus further reducing the activity. This study gave valuable input into the mechanisms of CO oxidation on sub-monolayer CoO films on Pt(111). However, the study was performed under low pressures and at RT, making it very different from realistic CO oxidation conditions.

To understand the contributions of various CoO phases on Pt(111) during such a catalytic process, steps toward bridging the before mentioned pressure gap are necessary. For this, it is necessary to study CoO_x/Pt(111) using in situ measurements at realistic temperatures and pressures. In **Paper I**, we exposed single-layer CoO_x islands supported on Pt(111) to CO, O_2 and 1:1 CO/O_2 mixture at 1 bar total pressure, at several elevated temperatures. By measuring Co K-edge XAFS spectra, we were able to follow changes in the chemical state and local structure of such films under ambient-pressure CO oxidation conditions.[47]

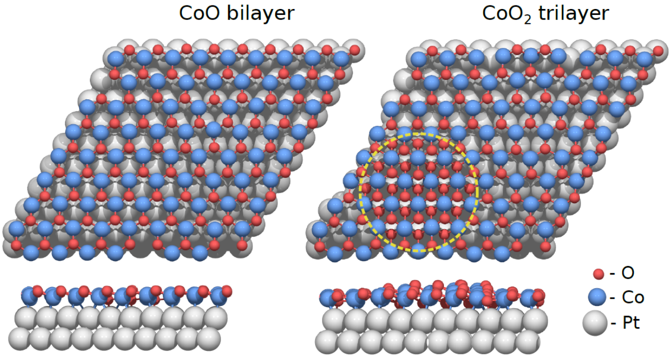

Figure 2.5: Top and side views of CoO bilayer structure (left) and CoO_2 trilayer structure (right, indicated by circle), after optimization with DFT.

2.2 FeO_x on Pt(111)

In catalysis, and especially in CO oxidation, iron oxide species were shown to be excellent promoters for Pt-based catalysts, which struggle with high catalytic activity at low temperatures.[48] There are many types of Pt-FeO catalysts, such as iron oxide-supported Pt nanoparticles, hybrid Fe(OH)-Pt NPs, single-atom Pt or Fe species[49,50], and ultra-thin iron oxides on Pt single crystal supports. A well studied model system is Pt/Fe_3O_4, which exhibits strong metal-support interactions between the Pt particles and the oxide support. When annealed in vacuum, Pt particles become encapsulated by a FeO(111) monolayer film which seems to be driven by the high adhesion energy between Pt and iron oxides.[51,52] Since this thesis aims to study ultra-thin oxide films as surface materials and their structural changes under ambient pressure conditions, the focus in on a ultra-thin iron oxide films supported on Pt(111) single crystals.

A thin film of bilayer FeO grown on Pt(111) single crystal was first described by Vurens et al.[53] in 1988. When FeO is deposited onto Pt(111) substrate, iron metal binds quite strongly to the platinum surface, exhibiting a hexagonal boron nitride-type structure with oxygen atoms buckled away from the surface.[54–56] This is shown in a model on the left-hand side of Figure 2.6. The lattice constant of FeO(111) (3.1Å) is around 12% larger than the lattice constant of Pt(111) (2.77Å), and a lattice mismatch between the two results in a characteristic moiré pattern observed both in the ball model and the LEED pattern (Figure 2.6 middle and right, respectively). It was shown by Sun et al.[57,58] that under oxygen-rich conditions, FeO film oxidizes to a trilayer FeO_2 phase with an additional oxygen layer intercalated between platinum support and iron layer (Figure 2.6, middle). The trilayer FeO_2 film was characterized by Johansson et al.[59] using XPS and LEED. They found that the FeO_2 also exhibits a moiré pattern, thus having an overall similar structure to the FeO bilayer. Upon subsequent CO exposure, the FeO_2 trilayer reduces back to the FeO bilayer.[60,61]

The activity of FeO_x/Pt(111) in oxidizing and reducing conditions, coupled with previous studies of iron oxides in CO oxidation, drives the desire to understanding the mechanism behind these processes on iron oxide thin films. Exposure of the 'bilayer' FeO phase on Pt(111) to CO/O_2 mixture revealed the activity of FeO_x/Pt(111) in CO oxidation at 450 K, the temperature at which pure platinum is inactive, and proposed high activity of the film due to contributions of oxygen from the FeO_2 trilayer in oxidation of CO to CO_2. Therefore, the low-temperature CO oxidation activity of FeO_x/Pt(111) is suggested to follow the Mars-van Krevelen type mechanism where CO reacts directly with oxygen from the trilayer film. So far, the evidence for this is provided by a combination of ex-situ characterization and near ambient pressure reactivity measurements.[62]

At around the same time, Fu et al.[63] studied CO oxidation over FeO islands on Pt(111) under UHV conditions. Saturation of the surface with CO, followed by O_2 exposure, led to the speedy conversion of CO to CO_2, a process not observed on pure Pt catalysts. The reaction rate was shown to be higher for smaller FeO islands compared to the bigger ones, which led to the conclusion that possibly edge sites of the Fe-terminated islands enable O_2 adsorption even when Pt surface is blocked by CO.

Years later, Zhang et al.[64] used DFT calculations and STM imaging of oxidized FeO films to study successive exposure to increasing doses of CO on the surface. Their findings suggested that the reaction occurs at the FeO/FeO_2 boundary, which is suggested to form under reaction conditions. DFT calculations identified the presence of reactive oxygen at said boundaries. Therefore, the group identified the trilayer FeO_2 phase as the crucial source of oxygen for the low temperature CO oxidation.

As it can be seen, there are different proposed mechanisms for CO oxidation over FeO_x/Pt(111). For a direct correlation between catalytic activity and FeO present phases, it is desirable to characterize the films during the reaction. So far, any evidence supporting the involvement of the trilayer phase has been provided solely by ex-situ measurements. With the motivation to gain a better understanding of the iron oxide phases present under CO oxidation conditions, **Paper II** focuses on *operando* XANES at the Fe K-edge to characterize present FeO_x phases on Pt(111) under CO oxidation conditions.

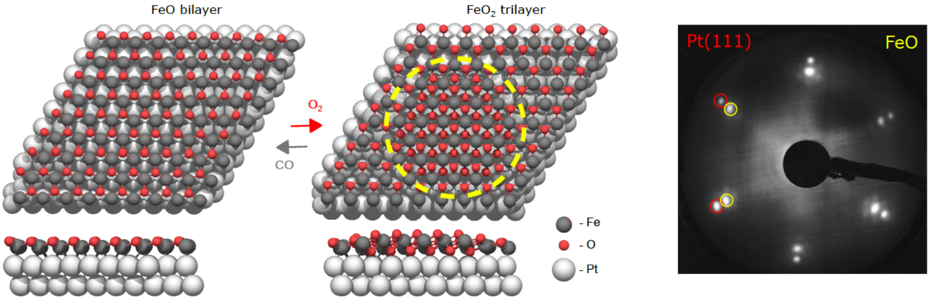

Figure 2.6: Top and side views of FeO bilayer structure (left) and FeO_2 trilayer structure (middle, indicated by circle). LEED pattern of FeO/Pt(111) (right).

2.3 Platinum-tin surface alloys

Pt_3Sn catalyst was shown to exhibit high catalytic activity for many reactions, such as alcohol electro-oxidation,[65–67] preferential CO oxidation (PROX) in H_2,[68,69] and low temperature CO oxidation,[70–73] where the promoting effect of Sn was attributed to electronic ligand effects.[74] Michalak et al.[75] performed an AP-XPS study, which revealed Sn oxide phase formation during CO oxidation over silica supported PtSn nanoparticles. This study suggested that the CO oxidation occurs at the interface between Pt and SnO_x domains, following a Mars-van Krevelen mechanism. Furthermore, it was experimentally and theoretically shown that CO binds less strongly to PtSn alloys then to bare Pt, indicating lower CO adsorption on the catalyst surface during reaction conditions, significantly reducing CO poisoning of the platinum. Furthermore, Axnanda et al.[71], exposed Sn(II) oxide grown on Pt(111) to CO, and found the correlation of the Sn(II) state and low-temperature CO oxidation activity. Their study also suggests that samples with lower oxide coverage, and therefore presumably higher specific edge densities, exhibited higher activity. The 2+ oxidation state of Sn has been suggested to be particularly important in the enhanced low-temperature CO oxidation activity of these catalysts.[71] However, the lack of spectroscopic evidence of the existence of the Sn 2+ phase keeps the reaction mechanism unclear.

For catalytic reactions over reducible oxides, the incorporation and release of oxygen at the oxide-metal boundary is of great importance. It was reported[76] that the less oxidized, (4 x 4) phase of tin oxide rapidly oxidizes to a (2 x 2n) phase under oxygen atmosphere, and it is equally easily reduced back under CO atmosphere. This transition is considered to be a potential explanation for the low temperature CO oxidation activity of platinum-tin. In order to shed a light on the CO oxidation reaction mechanism over Sn/Pt surface alloys, it is desirable to study them in operando, at realistic reaction conditions.

With this motivation, **Paper III** focuses on studies of Sn/Pt surface alloys in CO oxidation using GI-XANES. We show the formation of surface oxides during the exposure of the sample to 1:1 $CO:O_2$ mixture at 50 mbar and elevated temperatures.

2.4 NiMo-based oxides

The transition from fossil-based fuels to alternative feedstock, such as biofuels, is necessary to reach a net/zero carbon footprint. Fossil-based fuels are produced with hydrotreatment processes, such as hydrodesulfurization (HDS) for the reduction of sulfur and hydrodenitrogenation (HDN) for the reduction of nitrogen. The main difference between the alternative feedstock and fossil-based fuels is the biofuel's high oxygen content, which must be reduced to produce high quality fuels.

Molybdenum (Mo) is a well established catalyst for the hydrotreatment processes, and it is widely used in the petrochemical industry[77]. Mo-based catalysts are highly efficient in the hydrodeoxygenation (HDO) reaction for biomass, which makes them promising candidates for catalytic hydrotreatment of biomass instead of Pd and Pt catalysts, which are expensive and tend to be poisoned by sulphur[78]. The precursor for the Mo-based catalyst is the Mo oxide, which transforms into the active compound, Mo sulfide, when exposed to the sulfur containing feed-stock. In the slow change towards biofuels, some refineries today co-feed traditional fossil-based feedstock with the bio-based feedstock, making the environment in which the active Mo sulfide is produced much more oxidative, which in turn changes the sulfidation conditions and may result in a less active catalyst. Furthermore, the sulfidation into the active Mo sulfide strongly depends on the oxidation state and structure of the Mo oxide, where MoO_3 was shown to be more facile when compared to MoO_2.

Investigations on this catalytic system show that the active phase is the single-layer MoS_2 nanoclusters, whose edges are the active sites.[79–81] These active sites are linked to sulfur vacancies, which are responsible for creating reactive coordinated unsaturated sites (CUS) at the edges of the islands. Further improvement of the catalytic activity may be achieved by the addition of metal promoters, where the most popular options are Ni and Co. Specifically for the HDO processes, Ni has been the most effective candidate.[82–84] The role of Ni promoter is to donate electrons to Mo. Donated electrons will then weaken the bond to the sulfur, creating more CUS sites. The Ni:Mo ratio in a catalyst strongly affects its activity, and it is an important component to keep in mind when designing a catalyst for hydrotreating processes.

Another important parameter in the activity of Mo-based catalysts is the catalyst support, which will determine the size of the active MoS_2 islands.[85] Even though the most common support for such catalysts is the Al_2O_3, whose γ-phase[86] has a high surface area, a promising support is the δ-Al_2O_3[87,88] with its large pores, which may serve as an advantage in some hydrotreating processes. SiO_2 has also been studies as the possible support in order to further investigate the importance of the support-catalyst interactions.

Nickel and molybdenum based oxides were studied using XAFS as a part of this thesis, the results of this study are shown in **Paper V**. Catalysts studied in this project are industrial NiMo-based catalysts supported on δ-Al_2O_3 and SiO_2, as well as pure Ni and Mo metals supported on δ-Al_2O_3.

Chapter 3

Experimental Methods

This section will describe principles of ultra-thin film preparation, delicate sample transfer and three different measurements modes used in this work.

1 Sample preparation

Pt(111) supported ultra-thin films studied in this thesis are CoO_x, FeO_x and Sn/Pt surface alloys. All samples were prepared in UHV chambers with the base pressure in 10^{-10} mbar range, equipped with LEED, or RHEED optics. Figure 3.1 shows front and back views of the UHV system based at Malmö University in Malmö, Sweden.

Ultra-thin oxide films were prepared by reactive deposition of desired metal from an electron-beam evaporator in oxygen atmosphere. Sn/Pt alloys were prepared by electron-beam evaporation of the tin onto the platinum surface. Evaporation rate was determined using a quartz crystal microbalance (QCM) and the desired surface structure was confirmed by LEED or RHEED, depending on the sample and the UHV system used. Another UHV chamber was available for use in this work, and it is located at the Physics department at Lund University in Lund, Sweden. This UHV chamber is equipped with LEED, auger electron spectroscopy (AES) and STM. Prepared samples were transferred to this chamber using the vacuum suitcase to preserve the environment around the sample. AES was used to estimate the amount of metal and oxide on the surface of the material, and to confirm there were no contaminations on the surface. STM was used to confirm the morphology of the thin films.

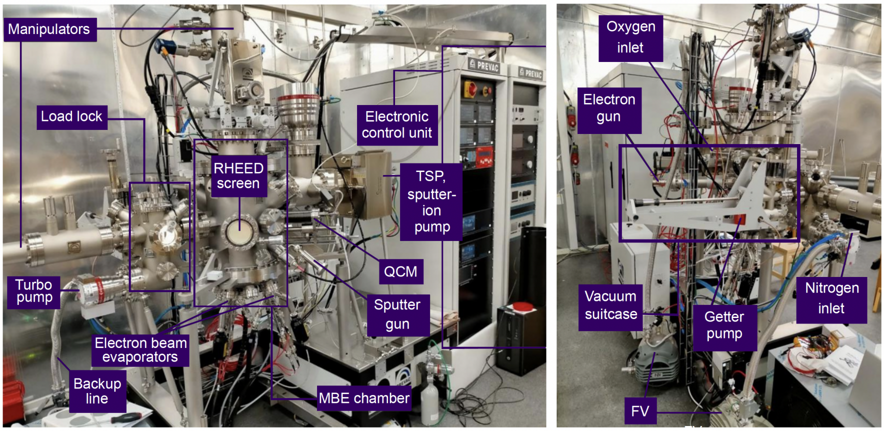

Figure 3.1: Front and back views of the UHV system at Malmö University in Malmö, Sweden.

2 Sample transfer

Ultra-thin film samples are prepared in an UHV chamber to control the structure of the film and to keep obtained structure pure. Since we aim to bridge the pressure gap and perform measurements outside of the UHV regime, we must take the sample out of the UHV chamber and load it into the appropriate environmental cell.

Taking the sample out of the UHV into the air exposes carefully grown ultra-thin film to many contaminants, which may adsorb on the surface and perhaps react with the film, resulting in changed surface structure. Therefore, it is desirable to transfer the sample in as clean as atmosphere as possible. An instrument allowing for that is called a vacuum suitcase. It can be seen on Figure 3.1a, that the vacuum suitcase is mounted to the load lock of the UHV system. The vacuum system has a getter pump which allows for the vacuum to be preserved even when the suitcase is disconnected from the UHV system.

Once the sample is ready, it is transferred to the vacuum suitcase and the valve between the suitcase and the load lock is closed. Then, the vacuum suitcase is disconnected from the system, and the sample is preserved in vacuum and ready for transfer to the beamline. Several things are required at the beamline for successful sample transfer from the vacuum suitcase to the environmental cell. A pumping station, with the vacuum suitcase attached to it as well as a small chamber are used to preserve the vacuum environment during the transfer between the suitcase and the small chamber. This is shown in Figure 3.2a. Once the pressure in the small chamber and the pumping station is satisfactory, the valve to the vacuum suitcase can be opened. Then, the sample is transferred from the vacuum suitcase to the small chamber by the use of both transfer arms. When the sample is secured in the small chamber, the valve between the small chamber and the pumping station must be closed in order for the small chamber to be disconnected from the system. The next step in the transfer process is to load the small chamber and the environmental cell into the glove box. The glove box is filled with argon gas, keeping water and oxygen concentrations lower than 1 ppm. In the glove box, the small chamber is opened and the sample is carefully mounted on top of the heater in the environmental cell. Figure 3.2b, c and d show mounting of the sample and the final result when the sample is secured in the environmental cell. Before the cell is taken out of the glove box, a graphite dome is mounted on top of the cell. The dome preserves the argon atmosphere inside the cell until the cell is connected to gas lines with He flow at the beamline end-station.

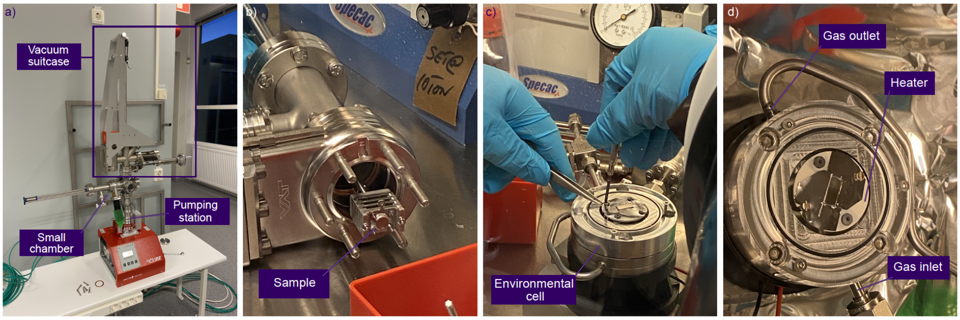

Figure 3.2: Transfer procedure using vacuum suitcase: a) pumping station with a vacuum suitcase and the small chamber. b) Small chamber with the sample, positioned in the glove box. c) Mounting of the in the environmental cell, graphite dome omitted. c) The sample mounted on top of the heater in the environmental cell, graphite dome omitted.

3 Fluorescence XAFS measurements

Fluorescence XAFS measurements in this work were performed at two different beamlines. Fluorescence XAFS on ultra-thin $CoO_x/Pt(111)$ was measured at P64 beamline at PETRA III in Hamburg, Germany, while fluorescence XAFS on ultra-thin $FeO_x/Pt(111)$ and on the Sn/Pt surface alloys were measured at the Balder beamline, at MAX IV synchrotron in Lund, Sweden.

Our first measurements of GI-XAFS were performed on the ultra-thin $CoO_x/Pt(111)$ catalyst. The experimental set up we used for these measurements is shown in Figure 3.3a. Here, an environmental cell with a beryllium dome is mounted, and sample alignment in the beam, as well as adjustment of the incidence angle are performed. Heating of the sample is done using a pyrolytic graphite/pyrolytic boron nitride heater, and the temperature is measured using a thermocouple mounted at the back of the crystal. The cell is connected to gas inlet and outlet lines which are used to flow inert gas, such as helium, to preserve as neutral environment as possible before the experiment begins, and to flow reaction gasses during the experiment. The passivated implanted planar silicon (PIPS) fluorescence detector is positioned in front of the dome.

Fluorescence GI-XAFS on ultra-thin $FeO_x/Pt(111)$ and on the Sn/Pt surface alloys was measured at the Balder beamline, at MAX IV synchrotron in Lund, Sweden, whose experimental set up is shown in Figure 3.3b and c. The same cell is used as in the previous measurements, as well as the mounting procedures. Once the sample is aligned in the beam, reactive gases are flown thorough the cell, the temperature of the sample is increased and XAFS measurements are performed using a germanium detector positioned in front of the dome.

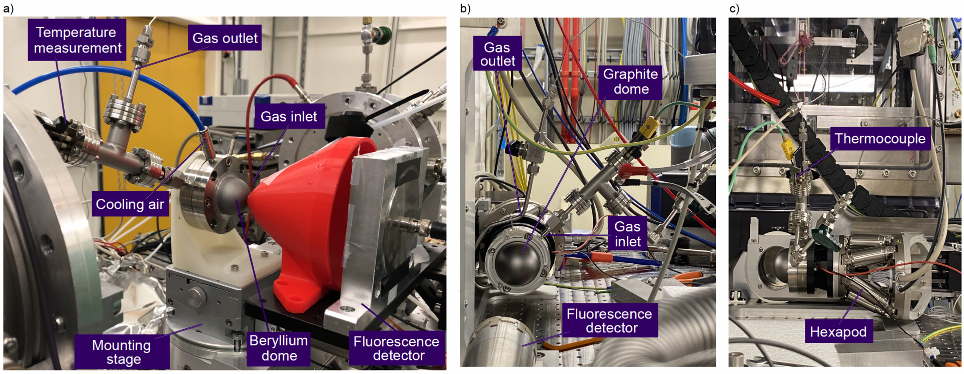

Figure 3.3: a) Fluorescence GI-XAFS experimental setup at the P64 beamline, at PETRA III, Hamburg, Germany. b)-c) Fluorescence GI-XAFS experimental setup at the Balder beamline, MAX IV, Lund, Sweden.)

4 Transmission XAFS measurements

Transmission mode of XAFS is used when it is possible for the X-ray to pass through the whole sample. One of the sample types measured in the transmission mode is a powder catalyst. In **Paper V**, NiMo based catalysts in powder form were studied in sulfidation reaction with transmission XAFS.

For this specific in situ transmission XAFS measurement, the catalyst is ground to a powder and loaded into a quartz capillary. The quartz capillary is then placed into a flow reactor cell, a thermocouple to measure the temperature is inserted into the capillary, and inlet and outlet gas lines are connected. At the beamline end-station, the reaction cell is places in front on the first ion chamber, and a hot air gun used for heating up the sample is placed under the cell. A mass spectrometer is installed at the outlet of the gas line to verify flow of the correct gases through the cell and to record the times at which gas changes occurred.

In this work, transmission XAFS measurements were performed at the ROCK beamline at Synchrotron SOLEIL in France. The Quick-XAS setup, characteristic for this beamline, allows for rapid jumps between two absorption edges due to two independent sets of monochromators and ion chambers. Figure 3.4 shows the experimental set up at the ROCK beamline.

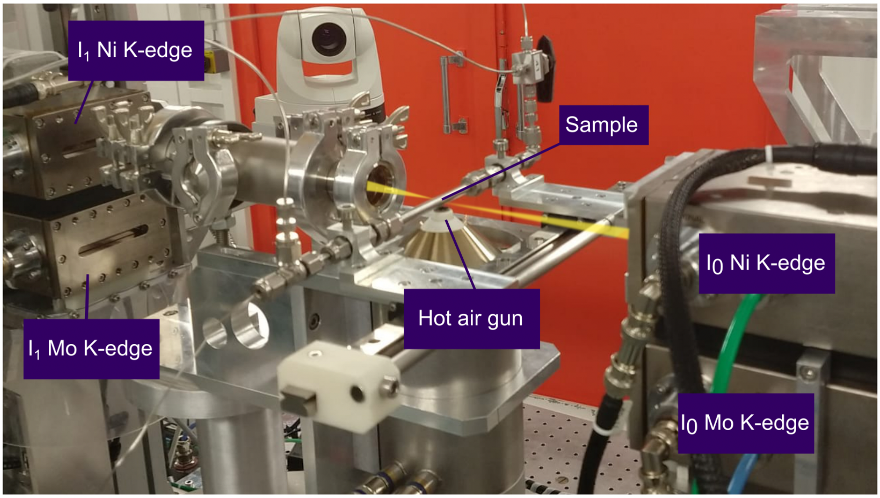

Figure 3.4: Transmission Quick-XAFS experimental set up at ROCK beamline at SOLEIL synchrotron in France.

5 Refle-XAFS measurements

Refle-XAFS is a mode of XAFS measurements where the intensity of the totally reflected beam is measured as a function of the incident beam energy.[89–93] Here, the sample is a mirror polished surface, and the incidence angle is set below the critical angle for total external reflection.[94] In **Paper IV**, we have used *operando* Refle-XAFS at P64 beamline at PETRA III in Hamburg, Germany, to study chemical surface changes of industrial alloys and model electrodes in harsh electrochemical environments.

For this purpose, hat shaped samples were mirror polished and placed in the PEEK (poly-ether ketone) EC flow cell. Figure 3.5 shows the EC mounted on the end station of the beamline. The cell is mounted on a linear and tilt stages which allow sample rotation to set the incidence angle. During the *operando* measurements, electrolyte was flown through the cell.

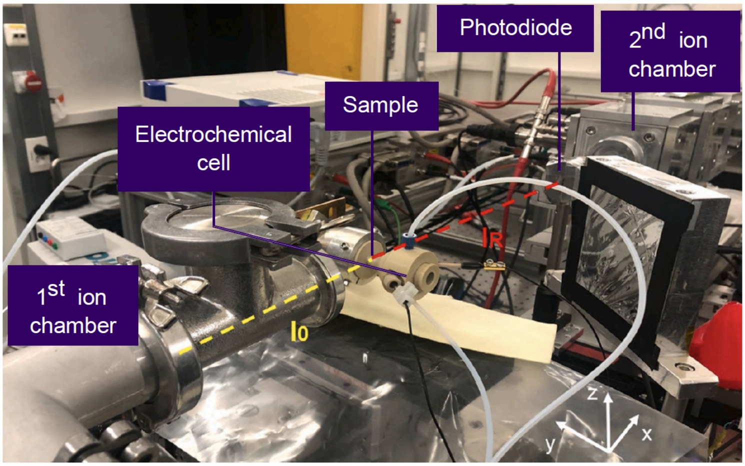

Figure 3.5: Operando Refle-XAFS experimental setup at the P64 beamline at PETRA III, DESY, Hamburg, Germany.

Chapter 4

Characterization Techniques

In order to fully characterize a catalyst surface, one would like to have the following information: which atoms are present on the surface, where are these atoms positioned, what is the concentration of the atoms, and what is the environment of these atoms, i.e., what are they bonded to.

Given the complexity of surface characterization, a single technique is insufficient. Therefore, my thesis employed a combination of methods. These included structural characterization techniques like low energy electron diffraction (LEED), reflection high energy electron diffraction (RHEED), and scanning tunnelling microscopy (STM), as well as chemically sensitive techniques such as auger electron spectroscopy (AES) and X-ray absorption fine structure (XAFS). Other techniques used in the papers included in the thesis were density function theory (DFT), X-ray photoelectron spectroscopy (XPS), atomic force microscopy (AFM) and X-ray reflectivity (XRR). This section will describe the operational principles, and experimental setups of the main techniques used in my work, which are LEED, RHED, STM and XAFS.

1 X-ray techniques

Traditionally, X-rays are generated using X-ray tubes in which electrons are accelerated towards a metal target.[95] A broadband spectrum of X-rays, called *bremsstrahlung*, is emitted when electrons decelerate within a metal target by deflection due to the interactions with electrons and nuclei, i.e. charged particles. Furthermore, atoms in the metal target can be excited and re-emit absorbed energy as electromagnetic radiation, which results in a sharp peak in the X-ray spectrum. These X-ray sources still find use in medical applications and laboratory based instruments.

Synchrotron radiation is a way of producing X-rays by accelerating electrons to a speed close to the speed of light, in facilities called synchrotrons. Synchrotrons are particle accelerators where electrons are stored and kept in a circular path in a storage ring. Outside of the storage ring, the electrons are generated in a linear accelerator to the desired speed before they are injected into the storage ring. A schematic of a storage ring with a linear accelerator is shown in Figure 4.1a. In order to produce a more intense X-ray beam, insertion devices are used in the straight parts of the storage ring. Both undulators and wigglers (shown in Figure 4.1b and c, respectively), are based on a series of magnets with alternating poles, where electrons are forced to sharply change their trajectory from a straight line into "wiggles". Wigglers use very powerful magnets which produce intense radiation over a wide spectral range by adding up the intensity of the emission cones inside the instrument. Since many experiments require a narrow range of wavelengths instead, undulators have been developed. Undulators use weaker magnets than wigglers which results in interference between photons which then emit coherent radiation with a wavelength determined by the period length of the undulator and the beam energy.[96] When it comes to many research areas today, such as studies of atomic surface or chemical changes during a reaction, synchrotron sources are superior to the classic X-ray tubes due to their ability to generate monochromatic and broadband radiation in the energy range from UV-light to hard X-rays, as well as its high photon flux, and the possibility to focus the X-ray beam to a tens of nanometer spot.[95] After the X-rays are generated by the insertion device, they enter the beamline part of the synchrotron, where the beam is further tuned to a specific experiment. The research in this thesis was performed at the MAX IV synchrotron in Lund, Sweden[97–99], at PETRA III, DESY in Hamburg, Germany[100,101] and at SOLEIL synchrotron in Saint-Aubin, France.[102,103]

Beamlines used in this work are:

- Balder beamline[104], at MAX IV, is a hard X-ray beamline with energies from 2.4 to 40 keV. This beamline is dedicated to X-ray absorption spectroscopy (XAS) and X-ray emission spectroscopy (XES), and its layout is shown in Figure 4.2. We have used this beamline in **Paper II** and **III**.
- P64[105], the "advanced XAFS" beamline at PETRA III, is a hard X-ray beamline with an undulator as an insertion device. The energy range of this beamline is from 4 to 45 keV and it is dedicated to XAFS experiments. We have used this beamline in **Paper I** where we used our own environ-

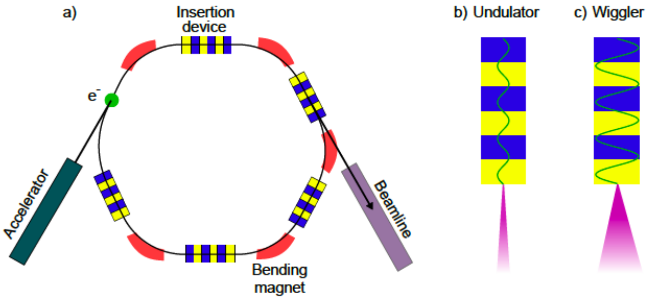

Figure 4.1: a) Schematic of an electron storage ring of a synchrotron with bending magnets, wigglers and undulators. b) Schematic illustration of an undulator insertion device. c) Schematic illustration of an wiggler insertion device.

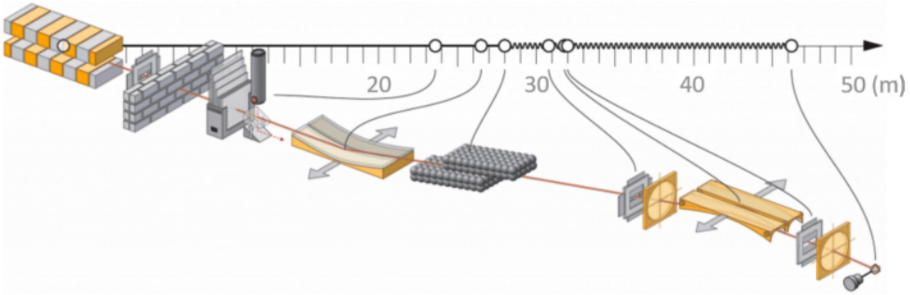

Figure 4.2: Illustration of the main elements in a synchrotron beamline, shown by the example of the Balder beamline at MAV IV laboratory. Adapted from reference.[104]

mental cell to measure in situ XAFS under ambient pressure conditions. Furthermore, in **Paper IV** we used our own electrochemical flow cell to measure operando Refle-XAFS under electrochemical conditions.

- ROCK beamline[106–108], at SOLEIL synchrotron, is a hard X-ray beamline with energies from 4 to 40 keV. This is a Quick-XAFS beamline which allows for rapid alteration between two different edges. This beamline was used in **Paper V** to follow transition from the oxide precursor to the active sulfide phase of a NiMo based catalyst during a sulfidation reaction.

1.1 X-ray absorption fine structure

X-ray absorption fine structure (XAFS) spectroscopy is an X-ray based technique that probes electronic and atomic local structures of different species in materials. XAFS is a very versatile technique that can be used on many different samples: solutions, powders, films, and pellets. Furthermore, it can be used in situ/operando as well as ex-situ. The possibility of using XAFS in situ/operando makes it a highly desirable technique in studying functional materials, which are a big part of our future. XAFS detects the local structure of the material, making it an ideal technique for studying small clusters that are part of large disordered systems. As XAFS is an element specific technique, it is capable of studying specific isolated events in a large, complicated material.

Traditionally, XAFS is separated into two parts: X-ray absorption near-edge structure spectroscopy (XANES) and extended X-ray absorption fine structure spectroscopy (EXAFS). XANES is sensitive to the formal oxidation state and the coordination chemistry of the atom in question, thus serving as a chemical fingerprint, while EXAFS gives structural information about distances, coordination number, and number of neighboring species to the absorbing atom.[109] Figure 4.3 shows XANES and EXAFS regions for an XAFS spectra of FeO(OH) measured at the Fe K-edge (E_0=7112 eV). XANES region is considered to be within around 50 eV of the absorption edge, while EXAFS region is found beyond this energy and up to 1000 eV above the edge or more.

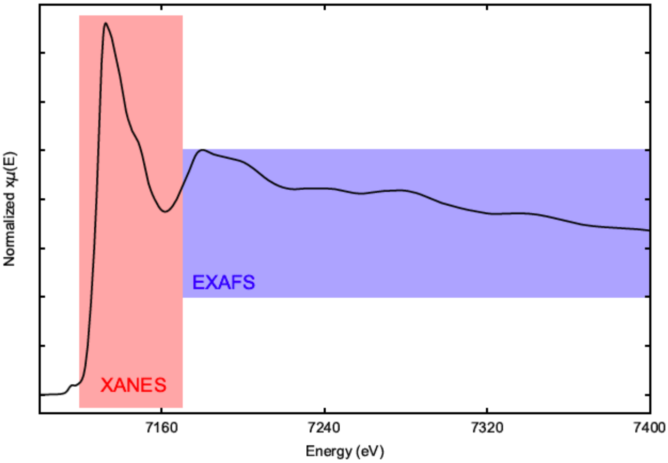

Figure 4.3: Measured XAFS spectrum of FeO(OH) with indicated XANES and EXAFS regions.

1.1.1 Basic operational principles

X-ray absorption spectroscopy (XAS) is performed by tuning the photon energy which is done by using a crystalline monochromator. XAS is based on the photoelectric effect, shown in Figure 4.4a, where an X-ray photon is absorbed by an electron in a core level, resulting in the ejection of an inner shell electron from the atom. For a core level to participate in the absorption event, the binding energy of it must be lower than the energy of the incident X-ray. Here, the

X-ray is absorbed and any excess energy of the binding energy is given to the photo-electron which is then ejected from the atom, creating a hole in the core level. The hole created by the photoelectric absorption can then be filled by two different processes. The first one is fluorescent X-ray emission shown in Figure 4.4b. Here, one of the outer shell electrons fills the hole, simultaneously creating a photon. The second process in Auger electron emission (Figure 4.4c) where the atom relaxes to its ground state by liberating an electron. When the incident X-ray has an energy equal to the binding energy of the core electron, a sharp rise in absorption is observed. This sharp rise is called an *absorption edge*. Depending on the core electron that gets excited in XAS, a different edge name is used. Principal quantum numbers n = 1, 2, 3 correspond to the K-, L-, and M-edges, respectively. Therefore, if 1s electron is being excited, we are looking at the K-edge, and if 2s or 2p electrons are being excited, we are looking at the L_1-, L_2- or L_3-edges. Figure 4.4d shows transitions and corresponding XAS edges.

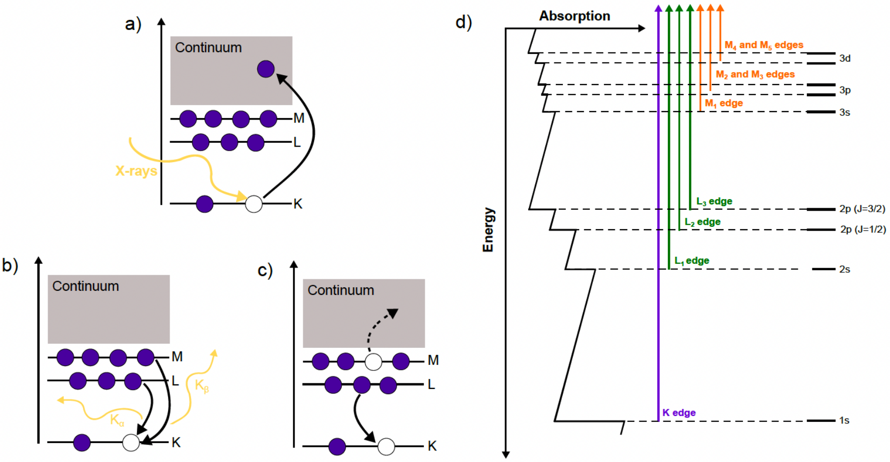

Figure 4.4: Schematic energy level diagrams of an atom. a) The photoelectric absorption process. An X-ray photon is adsorbed resulting in the ejection of an electron from the atom. The hole created in the shell can be filled by two processes: b) Fluorescent X-ray emission where one of the electrons of the outer shell fills the hole, creating a photon. c) Auger electron emission where the atom may relax to a ground state by liberating an electron. (X-ray book) d)Transitions and corresponding XAS edges.

The probability that X-rays will be absorbed by electron is given by the *absorption coefficient,* μ. The absorption coefficient is related to the incident and transmitted X-ray intensities through the Beer's Law is:

$$I = I_0 e^{-\mu x} \tag{4.1}$$

Where I_0 is the incident X-ray intensity, x is the thickness of the sample, and I is the intensity transmitted through the sample. In XAFS, one measures μ as a function of energy near and just above the energies of absorption edges. Since every atom has well defined binding energies of its core atoms, one can probe selected elements by tuning the X-ray energy to the adequate absorption edge. This is what makes XAFS an element specific technique. For XANES, one is interested in the oscillations at and around the absorption edge, but for EXAFS, oscillations far above the absorption edge are observed.

Absorption depends on an available state for the photo-electron, meaning there will be no absorption from a specific core level if there is no available state for the electron to fill. When there is a neighboring atom next to the adsorbing atom, the photo-electron will scatter from the electrons of the neighboring atom and return to the adsorbing atom. Therefore, the photo-electron scattered back from the neighboring atom will affect the absorption coefficient. This here, the scattering between neighboring atoms, is the origin of the *fine structure* of XAFS. Figure 4.5 shows a Fe K-edge XAFS spectra of bulk Fe_3O_4 where EXAFS contributions are highlighted. Since the EXAFS is proportional to the amplitude of the scattered photo-electron at the absorbing atom, constructive interference will result in a maximum in the spectra. In contrast, destructive interference will result in a minimum.

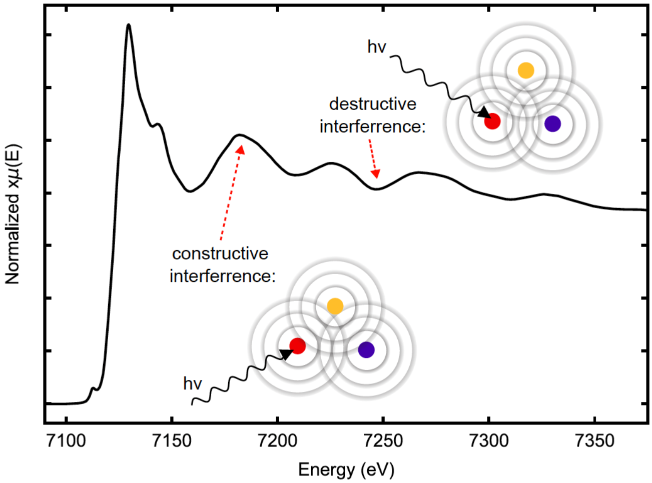

Figure 4.5: Fe K-edge XAFS spectra of bulk Fe_3O_4 with a schematic illustration of the origin of EXAFS oscillations.

The EXAFS fine structure, $\chi(E)$, is defined as:

$$\chi(E) = \frac{\mu(E) - \mu_0(E)}{\Delta\mu_0(E)} \tag{4.2}$$

where $\mu(E)$ is the measured absorption coefficient, $\mu_0(E)$ is a smooth background function representing the absorption of an isolated atom, and $\Delta\mu_0$ is the measured jump in the absorption at the threshold energy.[16] As mentioned above, EXAFS is explained in terms of wave behavior of the photo-electron created in the absorption process. Therefore, the X-ray energy is converted into the wave number of the photo-electron, k, which is defined as:

$$k = \sqrt{\frac{2m(E - E_0)}{\hbar^2}} \tag{4.3}$$

where E_0 is the absorption edge energy, m is the electron mass. Hence, $\chi(k)$ represents the oscillations as a function of photo-electron wave number, and it is referred to as "the EXAFS". As described above, the different oscillations in the EXAFS spectra correspond to different near-neighbor scatterings, which can be described using the EXAFS equation:

$$\chi(k) = S_0^2 \sum N_i \frac{f_i(k)}{kD_i^2} e^{\frac{-2D_i}{\lambda(k)}} \sin[2kD_i + \delta_i(k)] \tag{4.4}$$

where *f(k)* and *δ(k)* are scattering properties of the neighboring atoms of the excited atom, N is the number of neighboring atoms, R is the distance to the neighboring atom and σ^2 is the disorder in the neighbor distance. This equations allows for determination of N, R and σ^2 if scattering amplitude *f(k)* and phase-shift $\delta(k)$ are known.

1.1.2 Experimental setup

Transmission mode

There are several ways in which the X-ray absorption coefficient, *μ(E)*, can be measured. The simplest way is transmission. In transmission measurement, absorption is measured using equation 4.1.

As the X-ray penetrates through the sample, transmission mode requires the sample to be homogeneous, of appropriate thickness, and transparent to X-rays. If powder samples are measured, the grain size should not be much bigger than the absorption length. The transmission mode is appropriate for model compounds and elements with high concentrations. Figure 4.6a shows a schematic experimental setup for a transmission measurement, and Figure 4.6b shows a schematic of the XAFS setup at the beamline ROCK at Soleil, with a photo of the quartz capillary used as a reactor with a heating gun positioned underneath. The transmission mode experimental setup is fairly simple as all that is needed are two ion chambers to serve as I_0 and I_t detectors and a sample of thickness x which satisfies all requirements for such measurement.

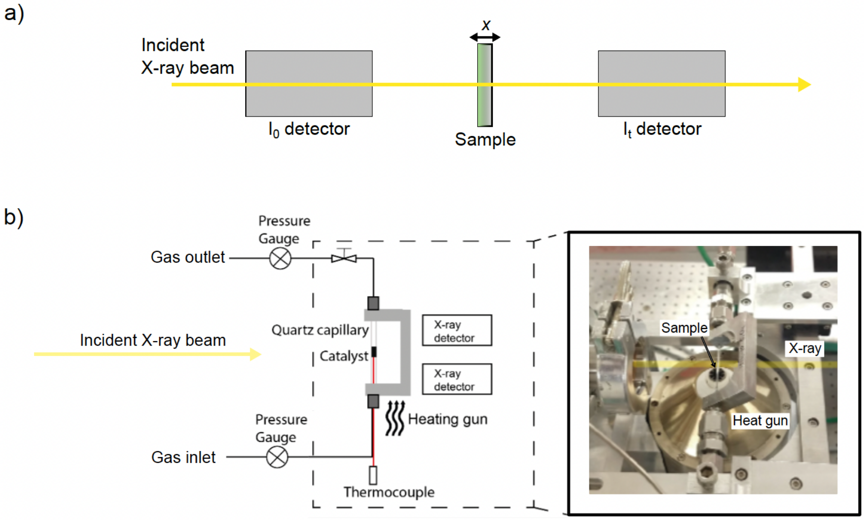

Figure 4.6: Transmission mode: a) Schematic representation of XAFS measurement in transmission mode with all elements included in the text. b) A schematic of the XAFS setup at the beamline ROCK at Soleil, with a photo of the quartz capillary used as a reactor with a heating gun positioned underneath.

Fluorescence mode

If the sample is too thick or perhaps has a very low concentration of the studied element, one has to use fluorescence mode to measure absorption coefficient, $\mu(E)$. When measuring in fluorescence mode, the X-rays emitted from the sample will contain fluorescent lines from the element of interest, fluorescent lines from other elements in the sample, as well as elastically and inelastically scattered X-rays. Fluorescence measurement can be represented by the equation:

$$\mu(E) \propto I_f/I_0 \tag{4.5}$$

where I_f is the fluorescent intensity measured by a fluorescence detector positioned at the specific angle compared to the sample, and I_0 is the incident X-ray intensity. Figure 4.7a and b show a schematic representation of a fluorescence measurement and photograph of the environmental cell containing a single crystal sample during a fluorescence measurement with a seven-element Germanium detector, taken at Balder beamline at MAX IV synchrotron in Lund, Sweden, respectively. In order to isolate fluorescent lines from the element of interest and, therefore, increase the signal-to-noise ratio, one can use physical or electronic methods. The physical method includes using a filter known as the Z-1 filter. The Z-1 filter is made out of the element with Z-1 relative to the element of interest. The goal of this filter is to absorb the scattering peak and only let it go through the fluorescent line of the element of interest. For example, when measuring at the Fe K_α edge, an Mn filter can be placed between the sample and the detector to absorb the scatter peak preferentially and only let through the Fe K_α line. In some of our experiments, when a PIPS detector was used, we used a filter of the element with Z-1 relative to the element we wanted to study. In other experiments, we used a seven-element germanium detector, which electronically performs energy discrimination on the measured X-ray emission spectra after the spectra have been collected.

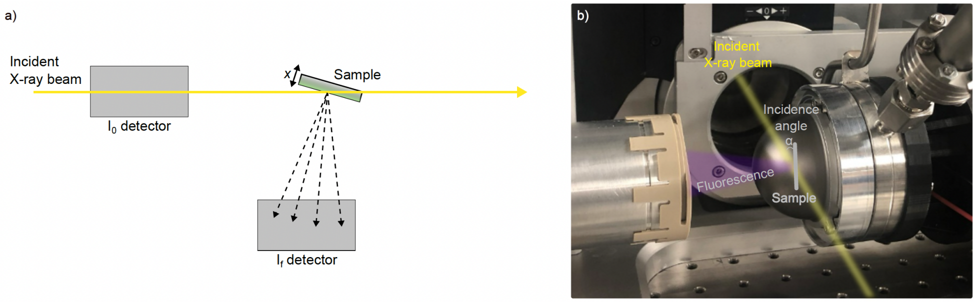

Figure 4.7: Fluorescence mode: a) Schematic representation of XAFS measurement in fluorescence mode with all elements included in the text. b) A photograph of the environmental cell containing a single crystal sample during a fluorescence measurement with a seven-element Germanium detector, taken at Balder beamline at MAX IV synchrotron in Lund, Sweden.

Grazing incidence geometry and Refle-XAFS

As previously mentioned, there are quite many requirements that samples have to have in order to be measured using XAFS. Everything discussed so far was based on the bulk samples since the technique has a large sampling depth due to the use of hard X-rays. For materials where the species of interest is found on the surface and where there are no bulk contributions, some modifications have to be made in order to achieve a sufficiently high signal-to-noise ratio. The use of *grazing-incidence geometry*, coupled with the fluorescence mode of signal collection, allows for the XAFS technique to be used on surfaces and interfaces.

In the grazing-incidence geometry, the incidence angle, α, is very small, resulting in a relatively small sampling volume at the surface of the sample. When the geometry is set near the critical angle, X-rays will have a very long path length with very little penetration into the crystal, meaning that very little of the signal will diffuse, leading to a very good signal-to-noise ratio. Figure 4.8a shows a schematic illustration of a GI-XAFS experimental set up. I_0 is the the incidence X-ray beam, the fluorescence signal from the thin film is detected by a SDD detector, and θ is the incidence angle of the X-ray beam. In this work, we reported surface sensitive characterization of CoO_x, FeO_x ultra-thin films, and Sn/Pt surface alloys with incidence angle smaller than 1°.

Refle-XAFS, on the other hand, utilizes an incidence angle below the critical angle for total external reflection.[94] Here, the reflected beam intensity is measured as a function of the incident beam energy.[92,110,111] In Refle-XAFS geometry, the reflectivity of the mirror polished surface is close to 100%, and surface chemistry and atomic structure details are revealed due to the energy dependent reflectance in the vicinity of a core-level absorption edge being dominated by XAFS features. Figure 4.8b shows a schematic illustration of a Refle-XAFS experimental set up, where I_0 is the incident X-ray beam, the totally reflected beam is measured via photodiode, and the incidence angle θ is below the critical angle for the measured material. In this work, operando Refle-XAFS was used to study chemical surface changes of industrial alloys and model electrodes in harsh electrochemical environments.

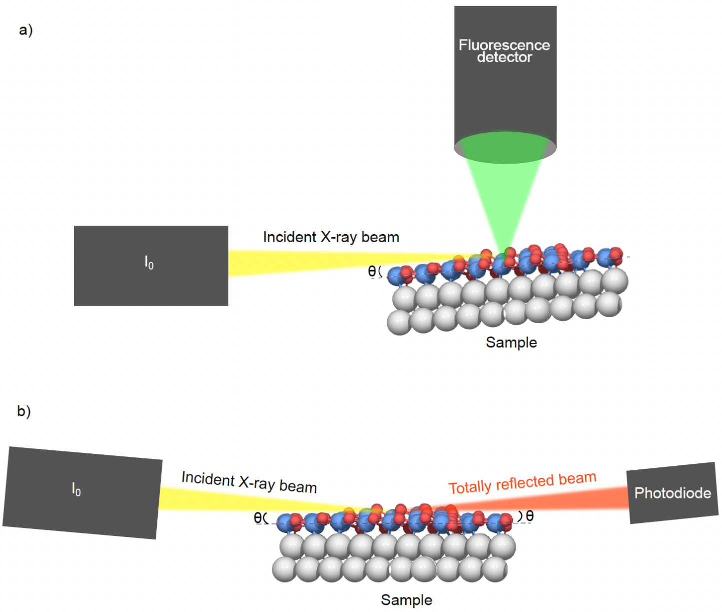

Figure 4.8: a) A schematic illustration of a GI-XAFS experimental set up will all elements described in the text. b) A schematic illustration of a Refle-XAFS experimental set up will all elements described in the text.

1.1.3 XAFS analysis

Data processing

No matter if the X-ray absorption coefficient, $\mu(E)$, is measured in transmission or fluorescence mode, the data processing follows the same steps. First, measured intensities are converted to the absorption coefficient, and all systematic measurement errors are corrected, such as self-absorption and detector dead-time. Second, a smooth pre-edge function from $\mu(E)$ is subtracted in order to get rid of background noise and absorption contributions from other edges. Third, the threshold energy, E_0, is identified as the energy of the maximum derivative of $\mu(E)$. Fourth, $\mu(E)$ is normalized to the range from 0 to 1. Spectra normalized until this step is used in XANES analysis. For EXAFS data analysis, further data processing steps are needed. First, the post-edge background is removed. Then, XAFS ($\chi(k)$) is isolated, and finally, $\chi(k)$ is k-weighted and Fourier transformed into R-space.[16] Graphical presentation of XAFS data processing steps is shown in Figure 4.9.

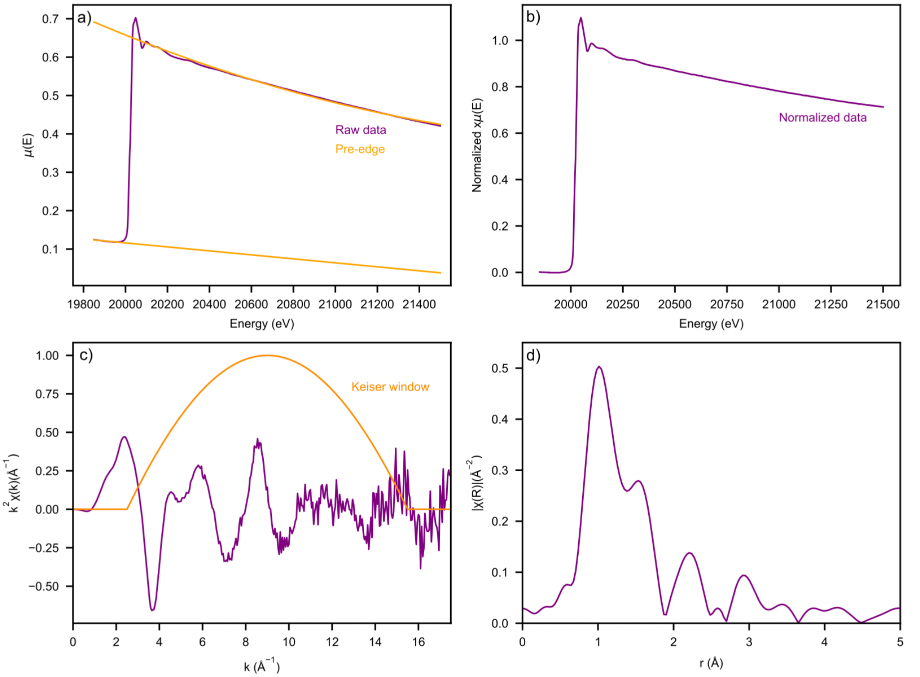

Figure 4.9: Mo K-edge spectra of NiMo supported on Al_2O_3 measured in transmission mode at ROCK beamline at SOLEIL Synchtron in Saint-Aubin, France. a) Raw data with pre-edge normalization lines. b) Normalized spectra. c) K-weighted EXAFS spectra with Keiser window shown. d) Fourier transform of the spectra in c) into R-space.

EXAFS fitting

Fitting of the EXAFS data is used for identification of nearest neighbors and estimation of bond lengths. In this section, I will explain steps and results of EXAFS fitting on the example of CoO thin films on Pt(111) substrate measured in fluorescence mode in various gas environments. Full data analysis and interpretation is found in Paper I.

To fit EXAFS data, it is customary to theoretically calculate scattering paths from known structures and use those to fit the measured spectra. In this case, Co-O and Co-Co scattering paths were calculated and used as references. The Larch[112] package was used to perform XAFS data processing and analysis, while IFEFFIT[113] implementation built into the Larch package was used for EXAFS fits.

Calculated theoretical scattering paths are then used in the EXAFS equation (see Equation 4.4) to obtain structural parameters from the measured data. Structural parameters of bond distance (R), coordination number (N), and mean-square-displacement (σ^2) are predicted during the fitting while energy (E_0) is changed until the best fit for $\chi(k)$ of the data is obtained. Fitting boundaries are defined both in k- and R-space and are chosen depending on the data quality.

In this work, EXAFS fitting was used in **Paper I** and **Paper V**. In **Paper I** and the case of CoO ultra thin films on Pt(111) under CO oxidation conditions, fitting was done in R-space using the data from k = 2.5 - 7.5 Å^{-1}1 and R = 1 - 4.5 Å. These conditions were chosen based on the data quality, which is significantly affected by the concentration of Co in the samples. However, the identification of nearest neighbors and estimation of bond lengths was successful. EXAFS fits for CoO_x/Pt(111) from **Paper I** are shown in Figure 4.10.

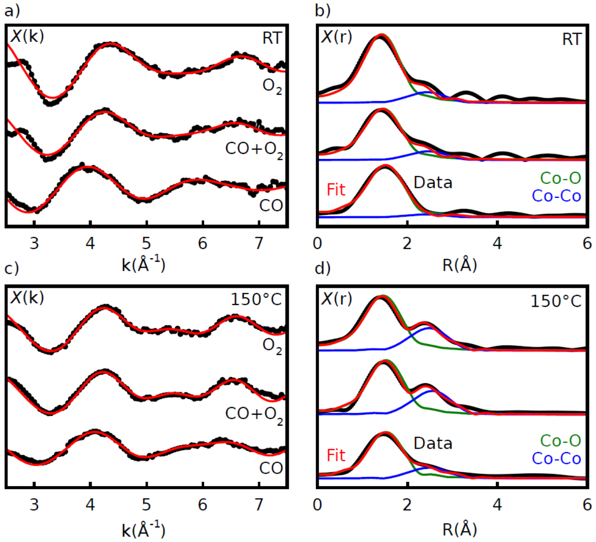

Figure 4.10: From **Paper I**: Raw EXAFS spectra and fits with specific scattering-path contributions for three gas flows at RT (a, b) and 150°C (c, d) from Paper I.

Linear combination analysis

Linear combination analysis (LCA) is a tool to quantitatively evaluate the spectra. In LCA, a set of standards is used to identify the composition of the recorded spectra.[114] A mathematical model is constructed, where each standard is multiplied by a coefficient and added to the result. The coefficient added to each standard represents the contribution of that standard to the sample. The calculations of all possibilities are calculated until a satisfactory fit to the measured data is obtained. For the LCA to be successful, references should be measured in as similar conditions as the unknown sample. Ideally, the sample and the references are measured at the same beamline, during the course of the same experiment, for easier energy calibration.

LCA was used in **Paper II** to analyze components of the FeO$_x$/Pt(111) spectra at different stages of the CO oxidation process. Previously measured spectra under pure O$_2$ and pure CO, together with spectra of metallic Fe foil, were used as references. LCA analysis of this experiment is shown in Figure 4.11. At the start of the experiment, the data is fitted very well with the 3+ iron component, indicating the oxidation state of iron at the beginning of the reaction to be 3+. At the onset of the reduction, at ~150 °C, a contribution of the 2+ component raises while that of the 3+ component reduces, indicating the change in the surface layer to a more reduced one. Furthermore, at the peak of reduction, at ~230 °C, the 2+ component is dominating the LCA fit. Finally, at the end of the experiment, the inclusion of the metallic component was necessary to obtain a good fit. The presence of metallic component on the surface indicated the destruction of the oxide film, probably due to high temperatures. This example shows how LCA can be used to gain a better understanding of the surface composition at various stages of the experiment.

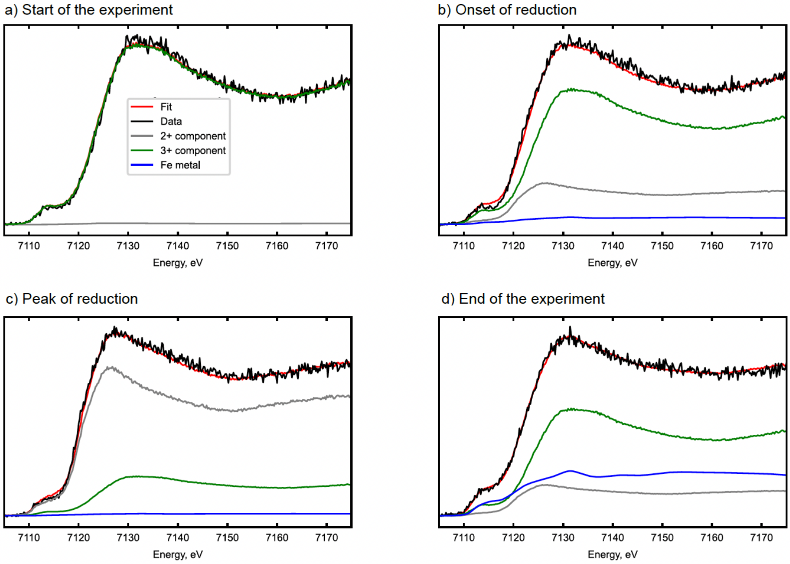

Figure 4.11: From **Paper II**: Linear combination analysis fits for the first temperature ramp over FeO$_x$/Pt(111). a) Fitted spectra at the start of the experiment. b) Fitted spectra at the onset of reduction. c) Fitted spectra at the peak of reduction. d) Fitted spectra at the end of the experiment.

2 Diffraction techniques

Electron diffraction is a technique used to determine the crystal structure by electron bombardment of a material, causing scattering off of the surface, which results in a diffraction pattern used to determine the atom arrangement in the studied material. Electron diffraction is based on elastic scattering, meaning that there is no energy loss and that wave vectors of the incident (k_0) and reflected (k_i) beam are unchanged. The wavelength of the incident, monochromatic beam is related to the wave vector as follows:

$$|k_0| = |k_i| = \frac{2\pi}{\lambda} \tag{4.6}$$

and in the case of an electron diffraction, the de Broglie wavelength if defined as:

$$\lambda(\text{Å}) = \frac{h}{\sqrt{2m_e \times E}} = \sqrt{\frac{150.6}{E(\text{eV})}} \tag{4.7}$$

where h is the Planck constant ($6.626 \times 10^{-3-}4$ $\text{m}^2\text{kg/s}$), m_e is the mass of an electron, and E is the kinetic energy of electrons. Elastically scattered electrons will leave the material and get collected by an appropriate detector. Their number, or the intensity of the reflected beam, is dependent by the inelastic mean free path of the electrons, expressed by:

$$I(x) = I_0 e^{-\dfrac{x}{\mu}} \tag{4.8}$$

where x is the distance electrons travel through a material without being inelastically scattered, I_0 is the initial flux of electrons and μ is the inelastic mean free path of electrons.[115] The surface sensitivity of a technique is determined by the inelastic mean free path of electrons, as well as their kinetic energy. LEED exhibits the lowest penetration depth of all UHV surface sensitive techniques because the inelastic mean free path is very small due to the high interaction of low energy electrons with matter.[116]

In order to observe a diffraction pattern, constructive interference of the outgoing electrons must take place. If one considers elastic scattering events only, constructive interference at an incident angle θ will take place when the atomic spacing, d_{hkl} is equal to an integer number of wavelengths, λ. This is shown graphically in Figure 4.12, and described by Bragg's law:

$$n\lambda = 2d_{hkl}sin\theta \tag{4.9}$$

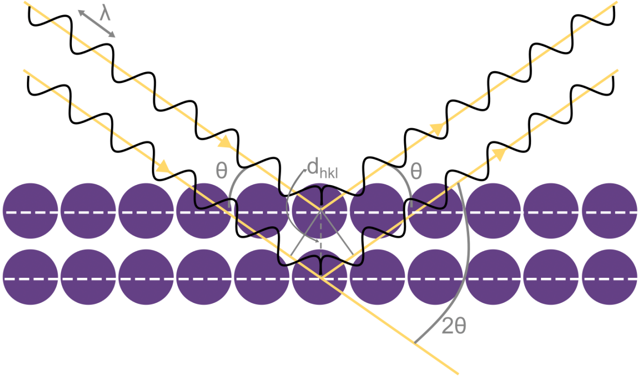

Figure 4.12: Scattering from a solid crystal resulting in constructive interference governed by Bragg's law.

Bragg's conditions for constructive interference can also be represented using von Laue's formulations, which state that the difference between the incident (k_0) and reflected (k_i) wave vectors is equal to the reciprocal lattice vector, G_{hkl} of the crystal.

$$k_i - k_0 = G_{hkl} \tag{4.10}$$

where the G_{hkl} is related to the d_{hkl} as follows:

$$|G_{hkl}| = \frac{2\pi}{d_{hkl}} \tag{4.11}$$

The previous equation shows the inverse proportionality between the reciprocal lattice vectors and the direct lattice vectors, whose direction is given by Miller indices, *h,k,l*, thus showing how diffraction experiments are used to obtain information about the real crystal lattice.

To further visualize the results of a diffraction experiment, one can construct an Ewald's sphere based on von Laue's formulations, and incident (k_0) and reflected (k_i) wave vectors. In electron diffraction, the length of the k-vector is defined by the electron gun energy. $|k_0|$ is the radius of the Ewald's sphere, and when the sphere intersects with the reciprocal lattice of the surface, the pattern will be visible on the fluorescent screen.[117] Figure 4.13 shows an illustration of an Ewald's sphere during RHEED experiment, when reciprocal space rods cross the Ewald's sphere, RHEED pattern will show streaks on the fluorescent screen.[117,118] The pattern observed on the fluorescent screen depends on the reciprocal space lattice.

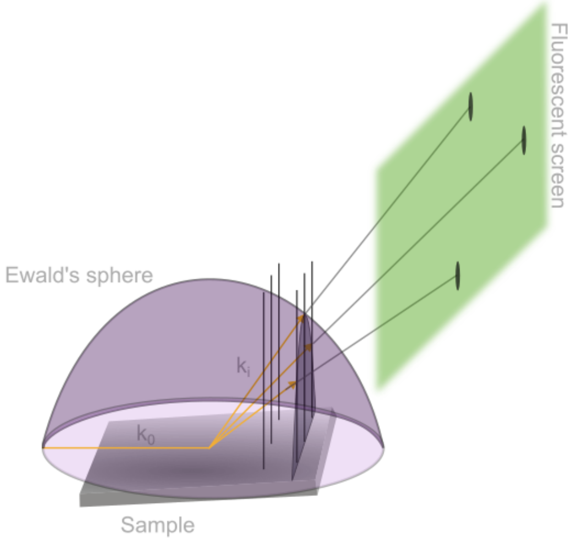

Figure 4.13: An illustration of an Ewald's sphere during Reflection High Energy Electron Diffraction (RHEED) experiment.

2.1 Low Energy Electron Diffraction

Low energy electron diffraction (LEED) is a surface science method most widely used for studying long range order single crystals.[119,120] The technique is based on material bombardment with a collimated beam of low energy electrons which produces a diffraction pattern in form of spots on a fluorescent screen. In this work, I used LEED to quickly and reliably check the surface order or disorder, and to confirm the uniformity of the surface. Here, I will briefly describe the basic operational principles of this method and its experimental setup.

2.1.1 Basic operational principle

LEED uses electrons with energy between 20 eV and 1000 eV which are elastically backscattered from a surface to provide its structural information.[121] These kinetic energies result in de Broglie wavelengths of 0.39 - 2.74 Å, which are needed to probe the surface layers of studied materials and will result in diffraction if atoms on the surface are arranged periodically.

The Bragg's law needs to be adjusted in the case of LEED, considering the in-plane lattice spacings along d_{hk} directions, as follows:

$$n\lambda = d_{hk} sin\theta \tag{4.12}$$

where θ is the angle between the normal of the surface and the reflected beam. In two-dimensional terms, von Laue's formulation can be defined as:

$$k_i - k_0 = G_{hk} = ha^* + kb^* \tag{4.13}$$

where a^* and b^* are reciprocal lattice vectors defined as:

$$a^* = 2\pi \frac{b \times \widehat{n}}{a(b \times \widehat{n})} \qquad b^* = 2\pi \frac{\widehat{n} \times a}{a(b \times \widehat{n})} \tag{4.14}$$

where $\widehat{n}$ is the surface normal unit vector. Figure 4.14 shows a schematic representation of Bragg diffraction with a perpendicular incident electron beam (a), a schematic representation od the atomic configuration of Pt(111) surface with a and b surface vectors (b) and a LEED image of Pt(111) surface with a^* and b^* reciprocal lattice vectors (c).

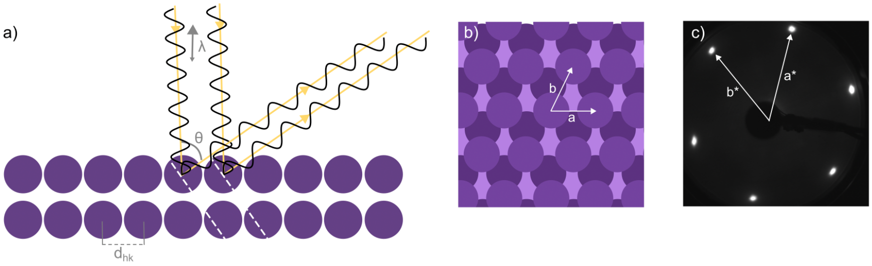

Figure 4.14: a) Schematic representation of Bragg diffraction with a perpendicular incident electron beam. b) Schematic representation of the atomic configuration of the Pt(111) surface with the corresponding surface lattice vectors. c) LEED image of an Pt(111) surface with the reciprocal lattice vectors included.

2.1.2 Experimental setup

A schematic of the LEED setup is shown in Figure 4.15. An electron gun generates a monochromatic electron beam, E_p, which interacts with the surface of the sample and diffracts. The sample must be conductive and grounded to prevent charging. For a diffraction pattern to be visible on a spherical fluorescent screen, elastically backscattered electrons have to undergo constructive interference. Backscattered electrons travel through a series of grids (G1 - G4 in Figure 4.15), which work together to direct the right electrons to the fluorescent screen. Grids G1 and G4 are grounded, and they ensure that the electrons travel in a field-free region. Grids G2 and G3 make sure that only elastically scattered electrons reach the detector. This is achieved by keeping electrons at a negative potential $V = - E_p + \Delta V$, where ΔV is in the range of 0 - 10 V. Finally, the fluorescent screen is biased at a high positive voltage (in our case, 6 keV) in order to accelerate the electrons enough so they can reach the kinetic energy necessary to trigger light emission in the detector. The diffraction pattern is then captured with a CCD camera or can be observed directly by the eye.

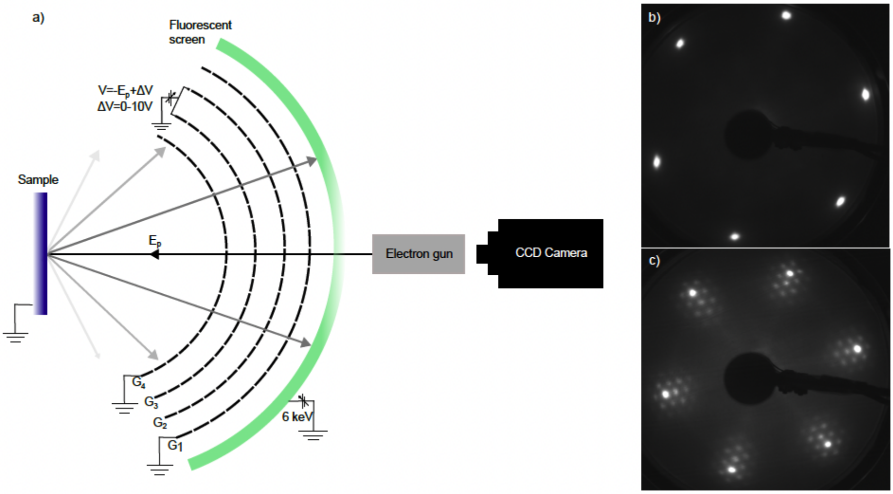

Figure 4.15: a) Schematic representation of LEED setup with all elements included in the text. b) LEED pattern of clean Pt(111) surface recorded at 54 eV. c) LEED pattern of CoO_x/Pt(111) recorded at 72 eV

2.2 Reflection High Energy Electron Diffraction

Reflection high energy electron diffraction (RHEED) is a surface science method most commonly used in MBE systems.[122] RHEED can be used to characterize crystalline structures, study surface quality, and chemical composition, and measure deposited materials' growth rate. The technique is based on material bombardment with a finely collimated beam of high-energy electrons, which produce a diffraction pattern in the form of rods or elongated spots on a fluorescent screen, representing a single direction on a crystal surface. Here, I will briefly describe the basic operational principles of this method and its experimental setup.

2.2.1 Basic operational principle

RHEED uses high energy electrons with energies between 10 keV and 100 keV with an incidence angle of 0.5° - 6°, depending on the desired penetration depth.[118] The grazing incidence of the incident electron beam makes RHEED highly sensitive to the surface structure, meaning that RHEED pattern provides fundamental information about the surface structure and morphology. Furthermore, the arrangement and spacing of the diffraction spots or rods in the RHEED pattern gives information on surface symmetry, real space lattice spacing and semi-quantitative information on types of surface defects. RHEED can also be used for quantitative analysis of reconstructed surfaces and surface disorder. Another great use of RHEED is to follow in situ growth of thin films, allowing for the determination of the number of atomic layers deposited and the growth mode of the film.

In this work, I used RHEED to determine the cleanliness of the Pt(111) surface, and to determine the crystal structure of the deposited films. By acquiring RHEED patterns at different azimuthal angles, I was able to map the reciprocal space structure of the surface. As an example, Figure 4.16a shows a reciprocal space map of Pt(111) surface (black spots) with an FeO thin film overlayer (red spots). Figure 4.16b and c show RHEED scans of clean Pt(111) surface acquired in two fundamental directions, Pt[11] and Pt[10]. Figure 4.16d shows RHEED scans of FeO/Pt(111) in Pt[11] direction, with arrows marking platinum and iron oxide features. I have used this type of analysis to determine the structure of the material, and in the case of the clean surface to determine the absence of the possible contaminants.

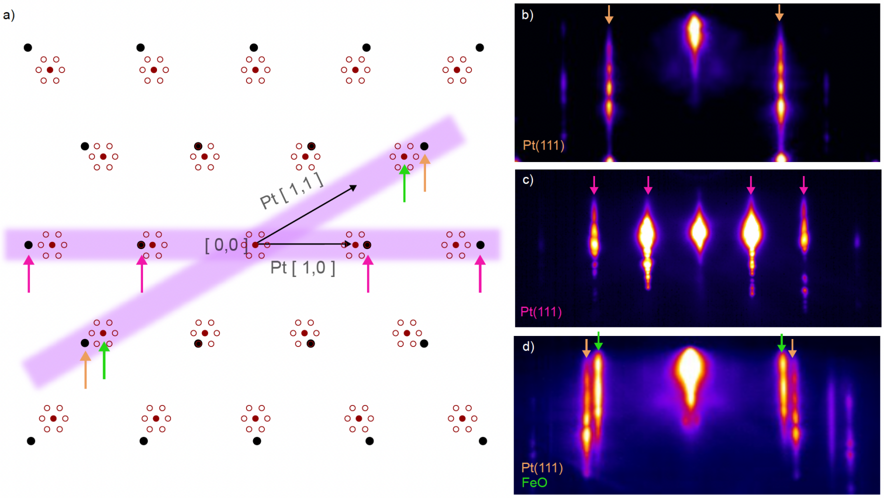

Figure 4.16: a) Reciprocal space map of FeO/Pt(111) surface with Pt[11] and Pt[10] directions indicated. b) RHEED pattern of clean Pt(111) surface obtained in Pt[11] directions, orange arrows showing matching reciprocal space points. b) RHEED pattern of clean Pt(111) surface obtained in Pt[10] directions, pink arrows showing matching reciprocal space points. C) RHEED pattern of FeO/Pt(111) surface obtained in Pt[11] directions, orange and green arrows showing matching reciprocal space points.

2.2.2 Experimental setup

A schematic of the RHEED setup is shown in Figure 4.17. An electron gun generates a finely collimated beam with high-energy electrons, which interacts with the sample and diffracts. The sample must have a pristine surface and be grounded to prevent charging. When constructive interference occurs, diffraction patterns are visible on the fluorescent screen. The angle of incidence of the electron beam is usually relatively low in order to penetrate only the topmost layers of the material. Typically, magnetic fields are used in a RHEED setup to change the incidence angle. In the RHEED experiment, it is very important to be able to rotate the sample along its azimuth. This rotation allows the user to adjust the diffraction angle and gain information about various surface sections. Once all diffraction conditions have been met, the naked eye sees the RHEED pattern on the fluorescent screen. A CCD camera captures it for easier data analysis and interpretation.

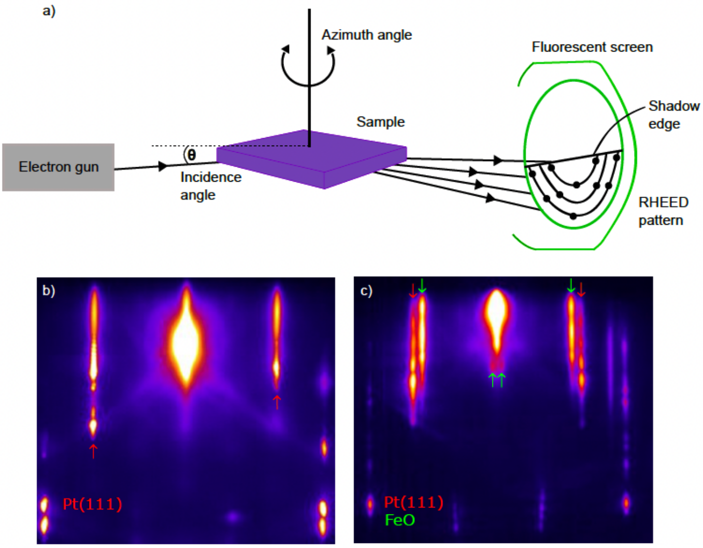

Figure 4.17: a) Schematic representation of RHEED setup with all elements included in the text. b) RHEED measurement of the clean Pt(111) surface along Pt[11] direction. c) RHEED measurement of the FeO_x/Pt(111) along Pt[11] direction.

3 Microscopy Techniques

3.1 Scanning Tunneling Microscopy

Scanning tunneling microscopy (STM) is an imaging technique which allows for the surface of a conductive material to be mapped out atom by atom in ultra-high resolution without the use of electron or light beams. In this work, I used STM to image prepared surfaces at atomic level and confirm the desired structure of those materials. Here, I will briefly describe basic operational principles of this method and its experimental setup.

3.1.1 Basic operational principle

The ”tunneling” in STM comes from quantum tunneling, which is the main concept of STM.[123,124] During the measurement, a sharp conductive tip is positioned very close to the surface of a conductive sample. A bias voltage is then applied, forcing the electrons to traverse the gap between the two. The tunneling current, which is a result of this process, is a function of the distance between the tip and the sample surface, applied voltage, and local density of states (LDOS) of the sample. While the tip scans the surface of the sample one line at a time, the intensity of the tunneling current maps out the sample's electronic density of states, which is then displayed as an image in the designated software.[125]

3.1.2 Experimental setup

STM has two basic operational modes: constant height mode and constant current mode. In my work, I used constant current mode. Constant height mode means that the distance between the position of the tip stays constant throughout the measurement. The changes in the tunneling current are then measured as a function of the tip position and bias voltage. This mode is usually used for very flat samples where the tip scans the surface very quickly, and there is little to no chance of the tip crashing into any structures on the surface of the sample.

The schematic representation of STM components is shown in Figure 4.18a. A tip, in this case made from Tungsten, is atomically sharp and mounted in the STM head, which is mounted on a piezo-electric tripod. All components are also indicated on a photograph from an STM, which I used in my work at the Physics Department of Lund University in Lund, Sweden. Tips are manufactured by electrochemical etching and can also be manipulated during the measurements by purposeful crashing into the surface or by applying voltage pulses. The piezo-electric tripod is used to control the movements of the tip on the surface of the sample. The highly accurate positioning of the tip is possible due to the expansions and contractions of piezo-electric materials with an applied current.

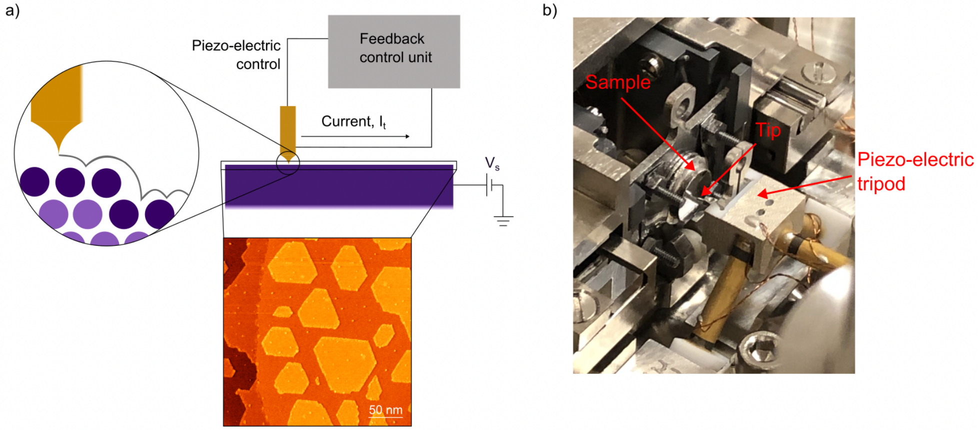

Figure 4.18: a) Schematic representation of STM components explained in the text. b) A photograph of an STM from Physics Department at Lund University, Lund, Sweden.

Chapter 5

Summary and Outlook

The thesis focused on the utilization of X-ray absorption fine structure spectroscopy to characterize various types of catalysts. The observations of structural changes of ultra thin oxides in CO oxidation under ambient pressure conditions on CoO_x/Pt(111), FeO_x/Pt(111) and Pt/Sn alloys and oxides, as well as the study of industrial NiMo-based catalysts in the sulfidation reaction using in situ Quick-XAFS on two different supports, and the use of Refle-XAFS to study industrial alloys and model electrodes in a harsh electrochemical environment, provide valuable insights and pave the way for future research in this field.

Paper I investigates structural changes of CoO_x/Pt(111) in CO oxidation. This study provides insight into the changes in the chemical state of Co - predominantly 2+ for CO-rich conditions and 3+ for O_2-rich conditions. These experiments demonstrate the power of hard X-ray spectroscopy to probe structures of well-defined oxide monolayers on metal single crystals under realistic catalytic conditions. Paper II further exploited the power of GI-XAFS on ultra thin oxide film. Here, monolayer FeO_x/Pt(111) was studied under ambient pressure CO oxidation conditions. The results of this study provide valuable insight into the unique properties of monolayer FeO during said conditions. Furthermore, the importance of Pt support for low temperature of CO oxidation over FeO_x thin films is highlighted. Paper III employs GI-XAFS in studies of well-known platinum-tin catalysts. Light is shed on the structure of these catalysts during CO oxidation conditions, which is related to theoretical calculations and previous studies using near ambient pressure X-ray photoelectron spectroscopy (NAP-XPS). This investigation shows the ability to use GI-XAFS at high X-ray energies, and it is the first step towards successful studies of PtSn fuel cell catalysts. A step further into bridging the materials and pressure gap was done in

Paper IV, where a Refle-XAFS study was done on industrial alloys and model electrodes. Here, the samples were exposed to a harsh electrochemical environment. The sulfidation of industrial NiMo-based catalysts on δ-Al_2O_3 and SiO_2 supports was studied in Paper V. The results provide insight into the effect of different parameters on sulfidation and the importance of NiMo interactions for hydrotreating industrial processes.

Improving data quality (signal-to-noise ratio) for further investigations using GI-XAFS on ultra thin oxides under realistic conditions will enable more detailed characterization of relevant phases. To aid the signal-to-noise ratio, we have improved the sample transfer from the UHV system to the beamline from Paper I to Papers II and III. From transport in the air, which maintained the CoO islands morphology, to a more delicate transfer using the vacuum suitcase, a pumping station, and a glove box, we managed to reduce the time samples were exposed to air. Furthermore, the detector used in the experiments plays a significant role in data quality. From a PIPS detector to a 7-element germanium detector, we improved the signal-to-noise ratio in XANES spectra. Since the goal is to investigate surface changes during a catalytic reaction, the sample's catalytic activity must also be followed. Further investigations would highly benefit from the activity measurements in situ, making it desirable to develop equipment in a way that will allow lower flow rates while keeping the desired conditions.

For further investigations of NiMo-based catalysts, the development of a model system representing the precursor phase, MoO_3, and studying from the fundamental perspective how such oxide behaves in sulfidation conditions could have significant implications. This could shed light on the mechanism of the activation of such catalysts. Furthermore, model systems with combinations of Mo and Ni atoms and their behavior in sulfidation would provide even more insight into the mechanism itself. Finally, exposing both industrial catalysts and potential model systems to organic molecules resembling those in the biofuel feedstock could provide insight into the complex processes taking place in the industrial reactors, opening up new avenues for research and development in this field.

Even though we have shown the promising potential of GI-XAFS in investigations of model and industrial systems in realistic conditions, we know that more than one technique is required to gain a complete picture of a process. Current and planned advances in modern synchrotrons worldwide are taking us a step closer to many dream experiments. One of those experiments has been showcased in Paper IV, where notoriously tricky solid-liquid interfaces in electrochemical reactors were possible to study by combining in situ XANES and electrochemical measurements, shedding light on the degradation mechanisms of electrocatalysts by gaining knowledge of the dissolution products found in the electrolyte.

To finalize, the quest for greener catalysts in CO oxidation is not only an academic pursuit; it holds the potential to revolutionize energy production and environmental impact. By understanding the atomic level processes on realistic surfaces, we open the door for more sustainable materials and processes. The insights gathered during this thesis, however small, can contribute to the innovations in both gas-phase and liquid-phase environments, ultimately contributing to a cleaner, more efficient energy future.

Chapter 6

References

[1] Cordus V. *Le guidon des apotiquaires. C'est à dire, la vraye forme et maniere de composer les médicamens ... / Traduite de latin en françoys, et repurgée.* Lyon: Cloquemin, 1575.

[2] Döbereiner J. W. Versuche Über di gährung. *Schweiger J.*, (20):213–214, 1816.

[3] Wisniak J. The history of catalysis. from the beginning to nobel prizes. *Educación Química*, 21(1):60–69, 2010.

[4] Kolasinski K. *Surface Science: Foundations of Catalysis and Nanoscience.* 03 2012.

[5] Che M. Nobel prize in chemistry 1912 to sabatier: Organic chemistry or catalysis? *Catalysis Today*, 218-219:162–171, 2013. Catalysis: From the active sites to the processes.

[6] Langmuir I. Chemical reactions on surfaces. *Trans. Fraday Soc.*, (17):607–620, 1922.

[7] Larsen H. and Chorkendorff I. From fundamental studies of reactivity on single crystals to the design of catalysts. *Surface Science Reports*, 35(5):163–222, 1999.

[8] Palmberg P. W. Ultrahigh vacuum and surface science. *Journal of Vacuum Science Technology A*, 12(4):946–952, 07 1994.

[9] Gabor A. Somorjai and Jeong Y. Park. Concepts, instruments, and model systems that enabled the rapid evolution of surface science. *Surface Science*, 603(10):1293–1300, 2009. Special Issue of Surface Science dedicated

to Prof. Dr. Dr. h.c. mult. Gerhard Ertl, Nobel-Laureate in Chemistry 2007.

[10] Nobel Prize Outreach AB. The Nobel Prize in Physics 1981. Nobelprize.org https://www.nobelprize.org/prizes/physics/1981/summary/ (accessed may 3, 2024).

[11] Nobel Prize Outreach AB. The Nobel Prize in Physics 1986. Nobelprize.org https://www.nobelprize.org/prizes/physics/1986/summary/ (accessed may 3, 2024).

[12] Nobel Prize Outreach AB. The Nobel Prize in Physics 1998. Nobelprize.org https://www.nobelprize.org/prizes/chemistry/1998/summary/ (accessed may 3, 2024).

[13] Nobel Prize Outreach AB. The Nobel Prize in Physics 2007. Nobelprize.org https://www.nobelprize.org/prizes/chemistry/2007/summary/ (accessed may 3, 2024).

[14] Peter Amann, David Degerman, Ming-Tao Lee, Mikhail Shipilin, Hsin-Yi Wang, Filippo Cavalca, Matthew Weston, Jörgen Gladh, Mikael Blom, Mikael Björkhage, Patrik Löfgren, Christoph Schlueter, Patrick Loemker, Katrin Ederer, Wolfgang Drube, Heshmat Noei, Johann Zehetner, Henrik Wentzel, John Åhlund, and Anders Nilsson. A high-pressure x-ray photoelectron spectroscopy instrument for studies of industrially relevant catalytic reactions at pressures of several bars. *The Review of scientific instruments*, 90:103102, 10 2019.

[15] Miquel Salmeron and Baran Eren. High-pressure scanning tunneling microscopy. *Chem. Rev.*, 121(2):962–1006, January 2021.

[16] Matthew Newville. *Fundamentals of XAFS.* University of Chicago, Chicago, IL, July 2004.

[17] Farrel W. Lytle. The EXAFS family tree: a personal history of the development of extended X-ray absorption fine structure. *J. Synchrotron Radiat*, 6(3):123–134, May 1999.

[18] D.C. Koningsberger, Barbara Mojet, Gert Van Dorssen, and D.E. Ramaker. Xafs spectroscopy: Fundamental principles and data analysis. *Top. Catal.*, 10:143–155, 05 2000.

[19] I. Chorkendorff and J.W. Niemantsverdriet. *Concepts of modern catalysis and kinetics.* Wiley-VCH Verlag, Germany, : 2., revised and enlarged edition edition, 2007.

[20] H.; Boudouard O. Le Chatelier. Limits of flammability of gaseous mixtures. *Bulletin de la Société Chimique de France*, 19:483–488, 1898.

[21] J. March. *Advanced Organic Chemistry: Reactions, Mechanisms, and Structure.* A Wiley-Interscience publication. Wiley, 1985.

[22] R. J. Baxter and P. Hu. Insight into why the Langmuir–Hinshelwood mechanism is generally preferred. *The Journal of Chemical Physics*, 116(11):4379–4381, 03 2002.

[23] H. Over, Y. D. Kim, A. P. Seitsonen, S. Wendt, E. Lundgren, M. Schmid, P. Varga, A. Morgante, and G. Ertl. Atomic-scale structure and catalytic reactivity of the ruo(2)(110) surface. *Science (New York, N.Y.)*, 287:1474–6, Feb 2000.

[24] Willem G. Onderwaater, Olivier Balmes, Sander B. Roobol, Matthijs Van Spronsen, Jakub Drnec, Francesco Carla, Roberto Felici, and Joost W.M. Frenken. Oxidation of co on pd(1 0 0): on the structural evolution of the pdo layer during the self sustained oscillation regime. *Catalysis, Structure and Reactivity*, 3(1-2):89–94, April 2017. Publisher Copyright: © 2017, © 2017 The Author(s). Published by Informa UK Limited, trading as Taylor Francis Group.

[25] M.Y. Gokhale and R.V. Mantri. Chapter 4 - api solid-form screening and selection. In Yihong Qiu, Yisheng Chen, Geoff G.Z. Zhang, Lawrence Yu, and Rao V. Mantri, editors, *Developing Solid Oral Dosage Forms (Second Edition)*, pages 85–112. Academic Press, Boston, second edition edition, 2017.

[26] Jing Zhang and J. Will Medlin. Catalyst design using an inverse strategy: From mechanistic studies on inverted model catalysts to applications of oxide-coated metal nanoparticles. *Surface Science Reports*, 73(4):117–152, 2018.

[27] Nataliia Petrova and Ivan Yakovkin. Mechanism of associative oxygen desorption from pt(111) surface. *The European Physical Journal B*, 58:257–262, 08 2007.

[28] G. M. Schwab and K. Koller. Combined action of metal and semiconductor catalysts. *J. Am. Chem. Soc.*, 90(12):3078–3080, June 1968.

[29] Gabor A. Somorjai and Jeong Y. Park. Molecular factors of catalytic selectivity. *Angewandte Chemie (International ed. in English)*, 47:9212–28, 2008.

[30] A. B. Boffa, C. Lin, A. T. Bell, and G. A. Somorjai. Lewis acidity as an explanation for oxide promotion of metals: implications of its importance and limits for catalytic reactions. *Catalysis Letters*, 27(3):243–249, 1994.

[31] S. J. Tauster, S. C. Fung, and R. L. Garten. Strong metal-support interactions. group 8 noble metals supported on titanium dioxide. *J. Am. Chem. Soc.*, 100(1):170–175, January 1978.

[32] S. J. Tauster. Strong metal-support interactions. *Acc. Chem. Res.*, 20(11):389–394, November 1987.

[33] Daniel Widmann and R. Jürgen Behm. Active oxygen on a au/tio2 catalyst: Formation, stability, and co oxidation activity. *Angewandte Chemie International Edition*, 50(43):10241–10245, 2011.

[34] Kwangjin An, Selim Alayoglu, Nathan Musselwhite, Sheba Plamthottam, Gérôme Melaet, Avery E. Lindeman, and Gabor A. Somorjai. Enhanced co oxidation rates at the interface of mesoporous oxides and pt nanoparticles. *Journal of the American Chemical Society*, 135:16689–96, Nov 2013.

[35] Carlos Hernández Mejía, Tom W. van Deelen, and Krijn P. de Jong. Activity enhancement of cobalt catalysts by tuning metal-support interactions. *Nature Communications*, 9(1):4459, 2018.

[36] Manon Bertram, Carolin Prössl, Michal Ronovský, Julius Knöppel, Peter Matvija, Lukáš Fusek, Tomáš Skála, Nataliya Tsud, Maximilian Kastenmeier, Vladimír Matolín, Karl J. J. Mayrhofer, Viktor Johánek, Josef Mysliveček, Serhiy Cherevko, Yaroslava Lykhach, Olaf Brummel, and Jörg Libuda. Cobalt oxide-supported pt electrocatalysts: Intimate correlation between particle size, electronic metal-support interaction and stability. *J. Phys. Chem. Lett.*, 11(19):8365–8371, October 2020.

[37] Yangyang Li, Yunshang Zhang, Kun Qian, and Weixin Huang. Metal-support interactions in metal/oxide catalysts and oxide-metal interactions in oxide/metal inverse catalysts. *ACS Catal.*, 12(2):1268–1287, January 2022.

[38] Tiancheng Pu, Wenhao Zhang, and Minghui Zhu. Engineering heterogeneous catalysis with strong metal–support interactions: Characterization, theory and manipulation. *Angewandte Chemie International Edition*, 62(4):e202212278, 2023.

[39] P. Thormählen, M. Skoglundh, E. Fridell, and B. Andersson. Low-temperature co oxidation over platinum and cobalt oxide catalysts. *J. Catal.*, 188(2):300–310, 1999.

[40] Jonas Jansson, Magnus Skoglundh, Erik Fridell, and Peter Thormählen. A mechanistic study of low temperature co oxidation over cobalt oxide. *Top Catal*, 16(1):385–389, September 2001.

[41] Heath Kersell, Zahra Hooshmand, George Yan, Duy Le, Huy Nguyen, Baran Eren, Cheng Hao Wu, Iradwikanari Waluyo, Adrian Hunt, Slavomír Nemšák, Gabor Somorjai, Talat S. Rahman, Philippe Sautet, and Miquel Salmeron. Co oxidation mechanisms on CoO_x-pt thin films. *J. Am. Chem. Soc.*, 142:8312–8322, 2020.

[42] Yu Tang, Lingjuan Ma, Jian Dou, Christopher M. Andolina, Yuting Li, Hongbin Ma, Stephen D. House, Xiaoyan Zhang, Judith Yang, and Franklin (Feng) Tao. Transition of surface phase of cobalt oxide during co oxidation. *Phys. Chem. Chem. Phys.*, 20:6440–6449, 2018.

[43] Hee Chan Song, Seungtaeg Oh, Sang Hoon Kim, Si Woo Lee, Song Yi Moon, Hanseul Choi, Soo-Hyun Kim, Yongman Kim, Jihun Oh, and Jeong Young Park. The effect of the oxidation states of supported oxides on catalytic activity: Co oxidation studies on pt/cobalt oxide. *Chem. Commun.*, 55:9503–9506, 2019.

[44] Chao Meng, Tao Ling, Tian-Yi Ma, Hui Wang, Zhenpeng Hu, Yue Zhou, Jing Mao, Xi-Wen Du, Mietek Jaroniec, and Shi-Zhang Qiao. Atomically and electronically coupled pt and coo hybrid nanocatalysts for enhanced electrocatalytic performance. *Advanced Materials*, 29(9):1604607, 2017.

[45] Jakob Fester, Michal Bajdich, Alex S. Walton, Z. Sun, Philipp N. Plessow, Aleksandra Vojvodic, and Jeppe V. Lauritsen. Comparative analysis of cobalt oxide nanoisland stability and edge structures on three related noble metal surfaces: Au(111), pt(111) and ag(111). *Top. Catal.*, 60:503–512, 2017.

[46] Jakob Fester, Zhaozong Sun, Jonathan Rodríguez-Fernández, and Jeppe V. Lauritsen. Structure of CoO_x thin films on pt(111) in oxidation of co. *J. Phys. Chem. C*, 123:17407–17415, 2019.

[47] Dorotea Gajdek, Pär A. T. Olsson, Sara Blomberg, Johan Gustafson, Per-Anders Carlsson, Dörthe Haase, Edvin Lundgren, and Lindsay R. Merte. Structural changes in monolayer cobalt oxides under ambient pressure co and o2 studied by in situ grazing-incidence x-ray absorption fine structure spectroscopy. *J. Phys. Chem. C*, 126(7):3411–3418, February 2022.

[48] Gang Liu, Andrew G. Walsh, and Peng Zhang. Synergism of iron and platinum species for low-temperature co oxidation: From two-dimensional

surface to nanoparticle and single-atom catalysts. *J. Phys. Chem. Lett.*, 11(6):2219–2229, March 2020.

[49] Qiang Fu, Wei-Xue Li, Yunxi Yao, Hongyang Liu, Hai-Yan Su, Ding Ma, Xiang-Kui Gu, Limin Chen, Zhen Wang, Hui Zhang, Bing Wang, and Xinhe Bao. Interface-confined ferrous centers for catalytic oxidation. *Science*, 328(5982):1141–1144, 2010.

[50] Suying Li, Gang Liu, Honglei Lian, Mingjun Jia, Guoming Zhao, Dazhen Jiang, and Wenxiang Zhang. Low-temperature co oxidation over supported pt catalysts prepared by colloid-deposition method. *Catalysis Communications*, 9(6):1045–1049, 2008.

[51] Z.-H. Qin, M. Lewandowski, Y.-N. Sun, S. Shaikhutdinov, and H.-J. Freund. Encapsulation of pt nanoparticles as a result of strong metalsupport interaction with fe3o4 (111). *J. Phys. Chem. C*, 112(27):10209–10213, July 2008.

[52] S. Shaikhutdinov and H.-J. Freund. Ultrathin oxide films on metal supports: structure-reactivity relations. *Annual review of physical chemistry*, 63:619–33, 2012.

[53] G.H. Vurens, M. Salmeron, and G.A. Somorjai. Structure, composition and chemisorption studies of thin ordered iron oxide films on platinum (111). *Surface Science*, 201(1):129–144, 1988.

[54] Y. J. Kim, C. Westphal, R. X. Ynzunza, H. C. Galloway, M. Salmeron, M. A. Van Hove, and C. S. Fadley. Interlayer interactions in epitaxial oxide growth: Feo on pt(111). *Phys. Rev. B*, 55:R13448–R13451, May 1997.

[55] Michael Ritter, Wolfgang Ranke, and Werner Weiss. Growth and structure of ultrathin feo films on pt(111) studied by stm and leed. *Physical Review B*, 57:7240–7251, 1998.

[56] Werner Weiss and Wolfgang Ranke. Surface chemistry and catalysis on well-defined epitaxial iron-oxide layers. *Progress in Surface Science*, 70(1):1–151, 2002.

[57] Ying-Na Sun, Zhi-Hui Qin, Mikolaj Lewandowski, Sarp Kaya, Shamil Shaikhutdinov, and Hans-Joachim Freund. When an encapsulating oxide layer promotes reaction on noble metals: Dewetting and in situ formation of an “inverted” feox/pt catalyst. *Catalysis Letters*, 126(1):31–35, November 2008.

[58] Y.-N. Sun, Z.-H. Qin, M. Lewandowski, E. Carrasco, M. Sterrer, S. Shaikhutdinov, and H.-J. Freund. Monolayer iron oxide film on platinum promotes low temperature co oxidation. *Journal of Catalysis*, 266(2):359–368, 2009.

[59] Niclas Johansson, Lindsay R. Merte, Elin Grånäs, Stefan Wendt, Jesper N. Andersen, Joachim Schnadt, and Jan Knudsen. Oxidation of ultrathin feo(111) grown on pt(111): Spectroscopic evidence for hydroxylation. *Topics in Catalysis*, 59(5):506–515, March 2016.

[60] Ying-Na Sun, Livia Giordano, Jacek Goniakowski, Mikolaj Lewandowski, Zhi-Hui Qin, Claudine Noguera, Shamil Shaikhutdinov, Gianfranco Pacchioni, and Hans-Joachim Freund. The interplay between structure and co oxidation catalysis on metal-supported ultrathin oxide films. *Angewandte Chemie International Edition*, 49(26):4418–4421, 2010.

[61] L. Giordano, M. Lewandowski, I. M. N. Groot, Y.-N. Sun, J. Goniakowski, C. Noguera, S. Shaikhutdinov, G. Pacchioni, and H.-J. Freund. Oxygen-induced transformations of an feo(111) film on pt(111): A combined dft and stm study. *The Journal of Physical Chemistry C*, 114(49):21504–21509, 2010.

[62] M. Lewandowski, I.M.N. Groot, S. Shaikhutdinov, and H.-J. Freund. Scanning tunneling microscopy evidence for the mars-van krevelen type mechanism of low temperature co oxidation on an feo(111) film on pt(111). *Catalysis Today*, 181(1):52–55, 2012. Frigyes Solymosi's special issue Planar Model System and Heterogeneous Catalysis.

[63] Qinglin Fu, Wei-Xue Li, Y. Yao, Holiday Liu, H.-Y Su, Ding Ma, X.-K Gu, L. Chen, Zhi-Gang Wang, Henggui Zhang, Boju Wang, and X. Bao. Interface-confined ferrous centers for catalytic oxidation. *Science*, 328:1141–, 01 2010.

[64] Ke Zhang, Linfei Li, Shamil Shaikhutdinov, and Hans-Joachim Freund. Carbon monoxide oxidation on metal-supported monolayer oxide films: Establishing which interface is active. *Angewandte Chemie International Edition*, 57(5):1261–1265, 2018.

[65] C Lamy, S Rousseau, E.M Belgsir, C Coutanceau, and J.-M Léger. Recent progress in the direct ethanol fuel cell: development of new platinum–tin electrocatalysts. *Electrochimica Acta*, 49(22):3901–3908, 2004. The role of electrochemistry in the sustained development of modern societies.

[66] Wei-Ping Zhou, Stephanus Axnanda, Michael G. White, Radoslav R. Adzic, and Jan Hrbek. Enhancement in ethanol electrooxidation by snox nanoislands grown on pt(111): Effect of metal oxide-metal interface sites. *J. Phys. Chem. C*, 115(33):16467–16473, August 2011.

[67] Wei-Ping Zhou, Wei An, Dong Su, Robert Palomino, Ping Liu, Michael G. White, and Radoslav R. Adzic. Electrooxidation of methanol at snox-pt interface: A tunable activity of tin oxide nanoparticles. *J. Phys. Chem. Lett.*, 3(22):3286–3290, November 2012.

[68] M. M. Schubert, M. J. Kahlich, G. Feldmeyer, M. Hüttner, S. Hackenberg, H. A. Gasteiger, and R. J. Behm. Bimetallic ptsn catalyst for selective co oxidation in h2-rich gases at low temperatures. *Phys. Chem. Chem. Phys.*, 3:1123–1131, 2001.

[69] Alina Moscu, Laurent Veyre, Chloé Thieuleux, Frederic Meunier, and Yves Schuurman. Co prox over pt–sn/al2o3: A combined kinetic and in situ drifts study. *Catalysis Today*, 258:241–246, 2015. Selected contributions in the field of heterogeneous catalysis and photocatalysis that were presented at the 8th International Conference on Environmental Catalysis (ICEC 2014).

[70] Céline Dupont, Yvette Jugnet, and David Loffreda. Theoretical evidence of ptsn alloy efficiency for co oxidation. *J. Am. Chem. Soc.*, 128(28):9129–9136, July 2006.

[71] Stephanus Axnanda, Wei-Ping Zhou, and Michael G. White. Co oxidation on nanostructured snox/pt(111) surfaces: unique properties of reduced snox. *Phys. Chem. Chem. Phys.*, 14:10207–10214, 2012.

[72] Stephanus Axnanda, Zhongwei Zhu, Weiping Zhou, Baohua Mao, Rui Chang, Sana Rani, Ethan Crumlin, Gabor Somorjai, and Zhi Liu. In situ characterizations of nanostructured snox/pt(111) surfaces using ambient-pressure xps (apxps) and high-pressure scanning tunneling microscopy (hpstm). *J. Phys. Chem. C*, 118(4):1935–1943, January 2014.

[73] Harald J. Wallander, Freddy E. Oropeza, Benjamin Hagman, Jan Knudsen, Edvin Lundgren, and Lindsay R. Merte. Oxidation of a platinum-tin alloy surface during catalytic co oxidation. *J. Phys. Chem. C*, 126(14):6258–6266, April 2022.

[74] Matthias Vandichel, Alina Moscu, and Henrik Grönbeck. Catalysis at the rim: A mechanism for low temperature co oxidation over pt3sn. *ACS Catal.*, 7(11):7431–7441, November 2017.

[75] William D. Michalak, James M. Krier, Selim Alayoglu, Jae-Yoon Shin, Kwangjin An, Kyriakos Komvopoulos, Zhi Liu, and Gabor A. Somorjai. Co oxidation on ptsn nanoparticle catalysts occurs at the interface of pt and sn oxide domains formed under reaction conditions. *Journal of Catalysis*, 312:17–25, 2014.

[76] Lindsay R. Merte, Nicolas Braud, Lars Buß, Malthe Kjær Bisbo, Harald J. Wallander, Jon Olaf Krisponeit, Jan Ingo Flege, Bjørk Hammer, Jens Falta, and Edvin Lundgren. Oxygen storage by tin oxide monolayers on pt3sn(111). *Journal of Physical Chemistry C*, 127(6):2988–2994, February 2023. Publisher Copyright: © 2023 The Authors. Published by American Chemical Society.

[77] Li Zeng and Chu Yong Cheng. A literature review of the recovery of molybdenum and vanadium from spent hydrodesulphurisation catalysts: Part i: Metallurgical processes. *Hydrometallurgy*, 98(1):1–9, 2009.

[78] Priscilla Souza, Raimundo Rabelo Neto, Luiz Borges, Gary Jacobs, Burtron Davis, Tawan Sooknoi, Daniel Resasco, and Fabio Noronha. Role of keto intermediates in the hydrodeoxygenation of phenol over pd on oxophilic supports. *ACS Catalysis*, 5:1318–1329, 01 2015.

[79] Rik V. Mom, Jaap N. Louwen, Joost W. M. Frenken, and Irene M. N. Groot. In situ observations of an active mos(2) model hydrodesulfurization catalyst. *Nature communications*, 10:2546, Jun 2019.

[80] Albert Bruix, Henrik Gøbel Füchtbauer, Anders K. Tuxen, Alexander S. Walton, Mie Andersen, Søren Porsgaard, Flemming Besenbacher, Bjørk Hammer, and Jeppe V. Lauritsen. In situ detection of active edge sites in single-layer mos2 catalysts. *ACS nano*, 9:9322–30, Sep 2015.

[81] Lars P. Hansen, Quentin M. Ramasse, Christian Kisielowski, Michael Brorson, Erik Johnson, Henrik Topsøe, and Stig Helveg. Atomic-scale edge structures on industrial-style mos2 nanocatalysts. *Angewandte Chemie International Edition*, 50(43):10153–10156, 2011.

[82] Edward Furimsky. Catalytic hydrodeoxygenation. *Applied Catalysis A: General*, 199(2):147–190, 2000.

[83] Henrik Topsøe, Bjerne S. Clausen, Nan-Yu Topsøe, and Per Zeuthen. Progress in the design of hydrotreating catalysts based on fundamental molecular insight. In D.L. Trimm, S. Akashah, M. Absi-Halabi, and A. Bishara, editors, *Catalysts in Petroleum Refining 1989*, volume 53 of *Studies in Surface Science and Catalysis*, pages 77–102. Elsevier, 1989.

[84] A. S. Koklyukhin, A. V. Mozhaev, V. A. Sal'nikov, and P. A. Nikul'shin. Promoter nature effect on the sensitivity of ni-mo/al2o3, co-mo/al2o3, and ni-co-mo/al2o3 catalysts to dodecanoic acid in the co-hydrotreating of dibenzothiophene and naphthalene. *Kinetics and Catalysis*, 58(4):463–470, 2017.

[85] Joaquín Brito and Jorge Laine. Characterization of supported moo3 by temperature-programmed reduction. *Polyhedron*, 5(1):179–182, 1986. PROCEEDINGS OF THE CLIMAX FIFTH INTERNATIONAL CONFERENCE.

[86] Jitendra Gangwar, Bipin Kumar Gupta, Surya Kant Tripathi, and Avanish Kumar Srivastava. Phase dependent thermal and spectroscopic responses of al2o3 nanostructures with different morphogenesis. *Nanoscale*, 7:13313–13344, 2015.

[87] Libor Kovarik, Mark Bowden, Arda Genc, János Szanyi, Charles H. F. Peden, and Ja Hun Kwak. Structure of δ-alumina: Toward the atomic level understanding of transition alumina phases. *J. Phys. Chem. C*, 118(31):18051–18058, August 2014.

[88] Xilong Wang, Zhen Zhao, Peng Zheng, Zhentao Chen, Aijun Duan, Chunming Xu, Jinqing Jiao, Honglei Zhang, Zhengkai Cao, and Binghui Ge. Synthesis of nimo catalysts supported on mesoporous al2o3 with different crystal forms and superior catalytic performance for the hydrodesulfurization of dibenzothiophene and 4,6-dimethyldibenzothiophene. *Journal of Catalysis*, 344:680–691, 2016.

[89] Hitoshi Abe, Yasuhiro Niwa, and Masao Kimura. A surface sensitive hard x-ray spectroscopic method applied to observe the surface layer reduction reaction of co oxide to co metal. *Phys. Chem. Chem. Phys.*, 22:24974–24977, 2020.

[90] Jin Suk Kim, Chang Hwan Chang, and Kyoo Young Kim. In situ x-ray absorption spectroscopic study of oxide film on fe alloy. *Physica Scripta*, 2005(T115):564, jan 2005.

[91] D. Hecht, P. Borthen, and H.-H. Strehblow. An x-ray absorption fine structure study of the initial stages of the anodic oxidation of silver. *Surface Science*, 365(2):263–277, 1996.

[92] Gerhard Martens and P Rabe. The extended x-ray absorption fine structure in the reflectivity at the k edge of cu. *Journal of Physics C Solid State Physics*, 14:1523, 11 2000.

[93] Dirk Lützenkirchen-Hecht and Ronald Frahm. Structure of reactively sputter deposited tin-nitride thin films: A combined x-ray photoelectron spectroscopy, in situ x-ray reflectivity and x-ray absorption spectroscopy study. *Thin Solid Films*, 493(1):67–76, 2005.

[94] U. Welzel, J. Ligot, P. Lamparter, A. C. Vermeulen, and E. J. Mittemeijer. Stress analysis of polycrystalline thin films and surface regions by X-ray diffraction. *Journal of Applied Crystallography*, 38(1):1–29, Feb 2005.

[95] Des McMorrow and J. Als-Nielsen. *Elements of modern X-ray physics.* Wiley, Hoboken, second edition edition, 2011.

[96] K. Wille. Introduction to insertion devices. In *CERN Accelerator School: Course on Synchrotron Radiation and Free-electron Lasers*, pages 61–75, 1996.

[97] Pedro F. Tavares, Simon C. Leemann, Magnus Sjöström, and Åke Andersson. The MAXIV storage ring project. *Journal of Synchrotron Radiation*, 21(5):862–877, Sep 2014.

[98] Nils Martensson and Mikael Eriksson. The saga of max iv, the first multi-bend achromat synchrotron light source. *Nuclear Instruments and Methods in Physics Research Section A: Accelerators, Spectrometers, Detectors and Associated Equipment*, 907:97–104, 2018. Advances in Instrumentation and Experimental Methods (Special Issue in Honour of Kai Siegbahn).

[99] Pedro F. Tavares, Eshraq Al-Dmour, Åke Andersson, Francis Cullinan, Brian N. Jensen, David Olsson, David K. Olsson, Magnus Sjöström, Hamed Tarawneh, Sara Thorin, and Alexey Vorozhtsov. Commissioning and first-year operational results of the max iv 3 gev ring. *Journal of Synchrotron Radiation*, 25(5):1291–1316, 2018.

[100] K Balewski. Commissioning of petra iii. in proceedings of 1st internationalparticle accelerator conference: Ipac. 2010. 2010.

[101] W. Drube, M. Bieler, W. A. Caliebe, H. Schulte-Schrepping, J. Spengler, M. Tischer, and R. Wanzenberg. The PETRA III extension. *AIP Conference Proceedings*, 1741(1):020035, 07 2016.

[102] Jean-Paul Ricaud, Pascale Betinelli, L Cassinari, Jm Filhol, B Gagey, Florent Langlois, and A Loulergue. Synchronization system of synchrotron soleil. 10 2007.

[103] A. Nadji. Synchrotron SOLEIL Upgrade Project. In *Proc. IPAC'21*, number 12 in International Particle Accelerator Conference,

pages 463–465. JACoW Publishing, Geneva, Switzerland, 08 2021. https://doi.org/10.18429/JACoW-IPAC2021-MOPAB131.

[104] Justus Just Susan Nehza3 Mahesh Ramakrishnan Dörthe Haase Stefan Carlson Stuart Ansell Kajsa Sigfridsson Clauss, Konstan3n Klemen3ev. Balder beamline, max iv beamline review report. Technical report, MAX IV laboratory, 2023.

[105] Wolfgang Caliebe, Vadim Murzin, Aleksandr Kalinko, and Marcel Görlitz. High-flux xafs-beamline p64 at petra iii. volume 2054, page 060031, 01 2019.

[106] Briois, V., Fonda, E., Belin, S., Barthe, L., La Fontaine, C., Langlois, F., Ribbens, M., and Villain, F. Samba: The 4–40 kev x-ray absorption spectroscopy beamline at soleil, 2011.

[107] E. Fonda, A. Rochet, M. Ribbens, L. Barthe, S. Belin, and V. Briois. The SAMBA quick-EXAFS monochromator: XAS with edge jumping. *Journal of Synchrotron Radiation*, 19(3):417–424, May 2012.

[108] Valerie Briois, C Fontaine, Stéphanie Belin, L Barthe, Th Moreno, Victor Pinty, A Carcy, R Girardot, and Emiliano Fonda. Rock: the new quick-exafs beamline at soleil. *Journal of Physics: Conference Series*, 712:012149, 05 2016.

[109] Qi Wang and Anatoly I. Frenkel. Chapter 5 - characterization of model nanocatalysts by x-ray absorption spectroscopy. In Paolo Fornasiero and Matteo Cargnello, editors, *Morphological, Compositional, and Shape Control of Materials for Catalysis*, volume 177 of *Studies in Surface Science and Catalysis*, pages 149–183. Elsevier, 2017.

[110] Dirk Lützenkirchen-Hecht, Jan Stötzel, Justus Just, Oliver Müller, Benjamin Bornmann, and Ronald Frahm. Time-resolved grazing incidence x-ray absorption spectroscopy for the in situ investigation of the initial stages of sputter-deposited copper thin films. *Physica Status Solidi (A) Applications and Materials Science*, 219(9), 2022. Publisher Copyright: © 2021 The Authors. physica status solidi (a) applications and materials science published by Wiley-VCH GmbH.

[111] G. Martens, P. Rabe, N. Schwentner, and A. Werner. Improved extended-x-ray-absorption fine-structure (exafs) studies applied to the investigation of cu-o, cu-n, and cu-br bond lengths. *Phys. Rev. B*, 17:1481–1488, Feb 1978.

[112] Matthew Newville. Larch: An analysis package for xafs and related spectroscopies. *Journal of Physics: Conference Series*, 430:012007, 04 2013.

[113] Matthew Newville. Ifeffit: interactive xafs analysis and feff fitting. *J. Synchrotron Radiat*, 8:322–324, 04 2001.

[114] Scott Calvin. *XAFS for Everyone.* 05 2013.

[115] M. P. Seah and W. A. Dench. Quantitative electron spectroscopy of surfaces: A standard data base for electron inelastic mean free paths in solids. *Surf. Interface Anal.*, 1(1):2–11, 1979.

[116] K. Bhavyasri, M. Sreshta, and R. Swethasri. Auger electron spectroscopy-a review. *Asian Journal of Pharmaceutical Research and Development*, 7:100–103, 06 2019.

[117] Shuji Hasegawa. *Reflection High-Energy Electron Diffraction.* 10 Hasegawa2012.

[118] Nassim Derriche, Simon Godin, Rysa Greenwood, Alejandro Mercado, and Ashley Nicole Warner. Reflection high-energy electron diffraction. 2019.

[119] S. Speller, W. Heiland, and M. Schleberger. Chapter 1 - surface characterization: Composition, structure and topography. In Hari Singh Nalwa, editor, *Handbook of Surfaces and Interfaces of Materials*, pages 1–53. Academic Press, Burlington, 2001.

[120] D.P. Woodruff. Low energy electron diffraction. In *Reference Module in Materials Science and Materials Engineering.* Elsevier, 2016.

[121] W. Moritz. Atomic structures of surfaces and interfaces. In Klaus Wandelt, editor, *Encyclopedia of Interfacial Chemistry*, pages 55–58. Elsevier, Oxford, 2018.

[122] Mark O'Steen, Eric Readinger, Stephen Farrell, Matthew Marek, Molly Doran, and Drew Hanser. Chapter 29 - systems and technology for production-scale molecular beam epitaxy. In Mohamed Henini, editor, *Molecular Beam Epitaxy (Second Edition)*, pages 649–675. Elsevier, second edition edition, 2018.

[123] Masaki Tsuji. 34 - electron microscopy. In Geoffrey Allen and John C. Bevington, editors, *Comprehensive Polymer Science and Supplements*, pages 785–840. Pergamon, Amsterdam, 1989.

[124] R.E. Smallman and A.H.W. Ngan. Chapter 5 - characterization and analysis. In R.E. Smallman and A.H.W. Ngan, editors, *Modern Physical Metallurgy (Eighth Edition)*, pages 159–250. Butterworth-Heinemann, Oxford, eighth edition edition, 2014.

[125] Srabanti Ghosh and Rajendra N. Basu. Chapter 4 - nanoscale characterization. In Satyabrata Mohapatra, Tuan Anh Nguyen, and Phuong Nguyen-Tri, editors, *Noble Metal-Metal Oxide Hybrid Nanoparticles*, Micro and Nano Technologies, pages 65–93. Woodhead Publishing, 2019.

Printed by Media-Tryck, Lund 2024 NORDIC SWAN ECOLABEL 3041 0903

LUND
UNIVERSITY

Department of Physics
Faculty of Science

ISBN 978-91-8104-131-6